

THE DYNAMIC APERTURE EXPERIMENT AT THE CERN SPS

W. Fischer, M. Giovannozzi and F. Schmidt

Abstract

The Dynamic Aperture Experiment at the CERN Super Proton Synchrotron (SPS) was aimed at finding the relevant effects that limit single-particle stability in hadron storage rings. These effects were studied in the SPS and compared with long-term particle tracking to determine to what extent computer simulations can predict the dynamic aperture under well-known conditions. Such investigations are very important for future hadron colliders like the Large Hadron Collider (LHC) as the design of these machines relies heavily on simulations. Besides this practical goal it was of utmost interest to improve the phenomenological understanding of the intricate details of particle motion in phase space. This experiment was carried out by successive teams over a period of ten years. The techniques, results, and conclusions are summarized in this report.

(Physical Review E Vol. 55, Nummer 3, p.3507)

Geneva, Switzerland
15 November 1995

Contents

1	INTRODUCTION	1
2	HISTORICAL OVERVIEW	2
2.1	<i>Experiments on transverse nonlinear dynamics</i>	2
2.2	<i>The SPS experiment</i>	2
2.2.1	Experimental session in 1986	2
2.2.2	Experimental session in 1988	3
2.2.3	Experimental sessions from 1989 to 1991	5
3	PREPARATION OF THE SPS AND ITS MODEL	8
3.1	<i>Instrumentation for the SPS experiment</i>	8
3.1.1	Data acquisition system BOSC	10
3.1.2	Wire scanners	14
3.2	<i>Experimental conditions</i>	17
3.3	<i>Tracking model and methods</i>	18
3.4	<i>Preparatory measurements</i>	19
3.4.1	Calibration measurements	19
3.4.2	Detuning with amplitude	19
4	THE SCRAPER EXPERIMENT	21
4.1	<i>Experimental results</i>	22
4.1.1	Intensity measurements	22
4.1.2	Discussion of diffusion models	23
4.1.3	Effect of two modulation frequencies	24
4.2	<i>Intensity curves obtained from numerical simulations</i>	26
4.2.1	Method of reconstruction	26
4.2.2	Error estimates	29
4.2.3	Results	29
5	THE WIRE SCANNER EXPERIMENT	30
5.1	<i>Beam profile measurements</i>	30
5.1.1	First working point - WP1	31
5.1.2	Second working point - WP2	32
5.2	<i>Dynamic aperture</i>	33
5.2.1	Measured	34
5.2.2	Computed	35
6	PHENOMENOLOGY OF CHAOTIC PARTICLE MOTION	36
6.1	<i>Simulation results</i>	36
6.2	<i>Experimental observations</i>	39
7	CONCLUSIONS	40
	ACKNOWLEDGMENTS	40
	REFERENCES	43

All high-energy hadron accelerators currently planned or under construction need superconducting technology to reach the high fields needed to guide and focus the beams. Whereas in the classic technology the required fields were reproduced by accurately shaping the magnetic pole pieces, in superconducting magnets the field quality depends almost entirely on the position and properties of the superconducting filaments inside the coils. As a result it is more difficult to avoid unwanted multipolar errors that affect the particle dynamics [1, 2].

Since hadrons lose a negligible part of their energy through synchrotron radiation, their motion in phase space can be adequately described in the framework of the Hamiltonian formalism. In such conservative systems, the nonlinearities can make the motion of the particles chaotic in parts of the phase space through which they slowly migrate outwards until they are lost at some obstacle in the beam pipe.

It is of utmost importance for the design of a machine like the Large Hadron Collider (LHC), the 7 TeV on 7 TeV proton collider planned in the Large Electron–Positron (LEP) tunnel at CERN, to understand in detail the nonlinear dynamics of the circulating particles. The main purpose of the dynamic aperture experiment at the Super Proton Synchrotron (SPS) was therefore to simulate a nonlinear machine including tune modulation, which is known to enhance the destabilizing effects of nonlinearities [3], and to investigate particle losses under these conditions.

The dynamic aperture, corresponding to the stable phase-space area, can be defined for our purpose as the maximum betatron amplitude below which no particle loss takes place within a time interval of interest. In the case of the LHC, the injection time is the relevant period since the transverse magnetic field errors attain large values and the particles have to stay at injection for 15 min with the beam size at its maximum. Unfortunately there is at present no tool or technique available to evaluate these loss times despite a decade of intense theoretical research. Hence, we have to rely on brute-force tracking. One of the main motivations for the experiments was to use the SPS as a test bench to compare experimental results from a controlled nonlinear machine with the predictions from tracking.

Answering this important practical problem was not the only incentive for the aperture studies. Much effort has been devoted to improving our phenomenological understanding of the intricate nature of nonlinear motion in phase space. We hope that theorists will find a consistent way to describe the slow-particle-loss mechanisms observed in the SPS experiment.

The next section puts our studies into context with experiments at other accelerator centers and gives a general overview of the results of the SPS experiment up to 1991. Section 3 describes the instrumentation, including its calibration, necessary for preparing the SPS machine. The experimental conditions, the tracking model, and preparatory experiments are stated as well. In Sec. 4 the experiment with scrapers is explained together with experimental and tracking results. The experimental dynamic aperture is compared with tracking results in Sec. 5. Finally, in Sec. 6, a detailed summary is given of all issues concerning our improved insight into nonlinear particle motion in hadron storage rings.

2.1 Experiments on transverse nonlinear dynamics

Transverse nonlinear resonance phenomena have been of interest to the accelerator community for many years (see Ref. [4]). With the planning of a new generation of large hadron colliders like the Superconducting Super Collider (SSC) and the LHC, intense experimental activity was started in the US at Fermilab, and in Europe at the CERN SPS and the DESY Hadronen Elektronen Ring Anlage (HERA) proton ring (see Refs. [5, 6, 7], respectively).

In the Fermilab E778 experiment [8] the measurements were predominantly made in the vicinity of the $2/5$ resonance. Various measurements were performed: detuning with amplitude, “smear” measurements, island capture (including tune modulation), and time-dependent beam profiles. The theoretical treatment relied on the Hamiltonian formalism, the phase diagram was studied in depth and the beam losses were described by a diffusive model.

In all experiments the sextupole magnets served as the dominant source of nonlinearities with the exception of the HERA experiment where the dynamic aperture due to the multipolar errors of the superconducting magnets was measured. In this experiment a good agreement between the tracking results (all known magnetic errors considered [7]) and the experimental measurements was achieved when the experimental conditions were well understood.

Dynamic aperture experiments have also been performed at the Indiana University Cyclotron Facility (IUCF) in which low-order resonances with and without tune modulation were studied and compared with Hamiltonian models (see Refs. [9] and [10]). At the Aladdin electron ring at the Synchrotron Radiation Center in Stoughton, Wisconsin, third-order resonances were studied [11] as well. The results were similar to those found in conservative systems since experimental periods were studied which were small compared to the damping time. More recently, studies have been started at the SPEAR storage ring at Stanford to analyze the full six-dimensional phase space [12].

2.2 The SPS experiment

The purpose of this section is to summarize the SPS experiments up to the end of 1991. We will restrict ourselves here to a discussion of the results while a thorough description of the experimental conditions will be given in the next section.

The early experiments can be grouped into three periods. In the initial phase [13] in 1986 the basic machine setup was defined and first short-term results were obtained. In 1988 the short-term dynamic aperture was studied in detail and a slow loss process was found [14]. From 1989 to 1991 an attempt was made [15] to understand this loss process quantitatively. To this end the experimental setup, the instrumentation, and the measurement and simulation techniques were revised. Some progress could be reported but reliable results have only been obtained in the period from 1992–1994. They will be discussed later.

2.2.1 Experimental session in 1986

The operational conditions of the SPS were carefully chosen so as to obtain a well-tunable but also very linear machine (see next section). With these conditions as a starting point, the SPS was made nonlinear in a controlled way with eight strong sextupoles. Two different configurations were tested: one leads to a strong excitation of the third-order resonance, a low-order resonance which is to be avoided for safe operation of a machine

with colliding beams; the other configuration suppresses this resonance so that the particle motion is dominated by higher order resonances. This has a greater resemblance to a machine like the LHC, which is very nonlinear due to the strong multipolar errors of its superconducting magnets. The latter configuration has been exclusively used for all following experiments. To test the dependence of nonlinear behavior on the strength of the sextupoles, two different current values were used. The higher value was taken just below the saturation level and the lower value was 1.8 times smaller. In all following experiments, except in 1988, we used the lower value because it provided a sufficiently high level of the nonlinearities at the chosen energy.

Wire scans were used to visualize a kicked beam: after one kick one finds the signature of a hollow beam filamented in phase space that shows a double-peak structure in the projection. A second kick partly restores the original one-peak structure that the beam had before the kick. Moreover, close to the third-order resonance the wire-scan profile is distorted revealing phase space deformations due to this resonance. Another important tool was the Schottky detector which allows a measurement of the tune distributions with a high resolution. With this instrument, losses due to particular resonances could be detected easily.

The experiment mainly studied the short-term dynamic aperture of various working points close to the fifth- and seventh-order resonances. This short-term dynamic aperture corresponds to a few seconds of SPS storage time or some 10^5 turns. In the tracking, with simulations over 10^2 to 10^3 turns the short-term dynamic aperture could be predicted quite well when the measured closed orbit and synchrotron oscillations were taken into account. Taking the simulations to 10^5 turns did not change the tracked dynamic aperture very much. The presence of a vertical closed orbit gave rise to skew resonances which led to particle loss when these resonances were approached in the experiment. As a consequence, in all following experiments, the closed orbit (in particular the vertical one) was carefully measured and corrected and whatever was left over after the correction was introduced in the simulations (see below). Moreover, some preliminary studies were done to understand the effect of a tune modulation ΔQ_x of some 10^{-3} .

Finally, long-term experiments (some minutes of storage time) were started without the synchrotron oscillations to avoid the additional effect due to the too strong RF noise. For the same reason we restricted all further studies to the four-dimensional phase space.

2.2.2 Experimental session in 1988

In this session two working points were studied close to the nest of coupling resonances of 5th and 7th order, respectively. The detuning with amplitude was measured and found to be in good agreement with tracking at those working points and also at the low and high sextupole excitation (see above). An example is shown in Fig. 1 which also shows that the border of chaotic motion, as determined in the tracking, fits well the amplitude where the short-term losses start to be visible in the experiment. As expected, this short-term dynamic aperture is smaller for the 5th order resonance which should have larger driving terms according to perturbation theory.

The conclusion was that the basic nonlinear parameters were well under control and that the short-term dynamic aperture can be well predicted by tracking. However, in the long-term study of this experiment a slow particle transport was found. The nature of this slow transport is still not fully understood and there are indications [16] that a simple model of diffusion is not sufficient to describe it. The experiment can be described as follows (see Fig. 2): at the beginning the lifetime is about 75 min, then a scraper is

moved in till the lifetime is reduced to 40 min. After a minute the scraper is retracted by 3 mm which results in a period of roughly 1 min in which almost no losses are detected. It seems that this is the time the particles need to “diffuse” out till they reach the retracted scraper. Thereafter one finds that the lifetime stabilizes at 65 min which is close to the original value. Finally, the lifetime of 36 min is recorded (which is close to the 40 min after the first scraping) when the scraper is put back to its closest location with respect to the beam center. From this a “diffusion” rate of 3 mm per minute can be calculated. It goes without saying that the SPS was also studied without strong sextupoles: no “diffusion” could be found in that case.

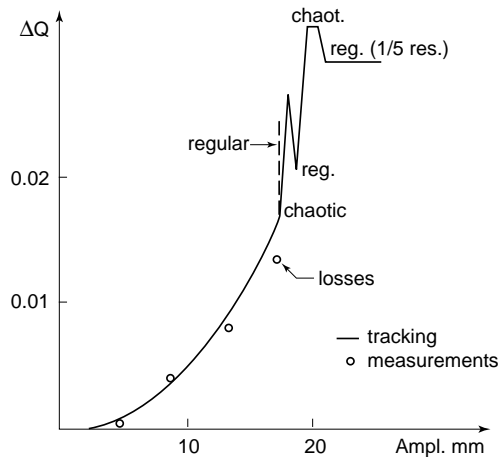


Figure 1: Comparison of tracking with experiment (close to 5th order resonance).

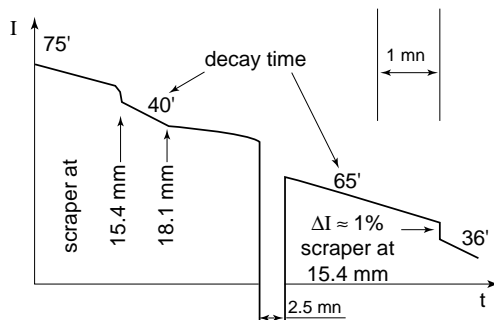


Figure 2: Detection of slow “diffusion”.

One of the goals of the SPS experiment was to establish a criterion of stability for the LHC. The whole concept of such a stability criterion has been subject to controversial discussions, a summary of which is given in Appendix A. It is shown there as well that the stability criterion is violated by the measured “diffusion” rate. This reduction of the long-term dynamic aperture cannot be easily explained by tracking. In fact, in the same amplitude range, the tracking predicts regular (and therefore completely stable) motion. A rather strong effect is clearly left out. A good candidate to explain this effect is the power supply ripple that causes a tune modulation which, in conjunction with the nonlinearities, may reduce the dynamic aperture. In the tracking [17] such an effect on the dynamic aperture is found when the tune modulation depth is of the order of some 10^{-3} . The same study also finds that in the range of tune modulation frequencies between 10 Hz

and 600 Hz, the smaller frequencies are much more dangerous than the larger ones. It has been demonstrated that this effect does not vanish for a different working point or another sextupole configuration. Moreover, it has been shown that the effect of a modulation due to a large number of elements can be well approximated by one single element when its strength is adjusted accordingly.

2.2.3 Experimental sessions from 1989 to 1991

The 1988 experiments and the theoretical studies led to the understanding of slow particle losses in a qualitative manner. Moreover, it was confirmed in an independent experiment in 1989 at Fermilab [18] that the combined effect of tune modulation and nonlinearities leads to a strong reduction of the dynamic aperture. In the following years we performed our experiments with a view to measuring “diffusion” rates as a function of betatron amplitude, of tune modulation depth (larger than the natural one), and of tune modulation frequency. It turned out, however, to be much more difficult than expected to get quantitative and reproducible results from the experiment.

It was realized that a much better control of the machine parameters was needed and that the measurement techniques had to be reviewed. The closed orbit, in particular the vertical one, had to be corrected to extremely low values. The linear coupling as well as the chromaticity were corrected to the best levels possible. It also became clear that the beam in the SPS had to be considered as a distribution of particles rather than a pencil beam. This remained true even with all these careful machine adjustments in place and after removing the tails of the distribution with scrapers. To sample a certain betatron amplitude it was therefore necessary to use a single kick instead of heating the beam with many small kicks. Moreover, it became mandatory to apply the same measurement procedure each time in order to arrive, at least approximately, at reproducible transverse distributions of protons. The problem of knowing the precise particle distribution also made it very difficult to draw conclusions from lifetime measurements. Finally, we found that the range of amplitudes of interest was of the order of the width of the distribution, which further complicated the interpretation of the results. This range of amplitudes is defined on the upper side by the smallest amplitude at which the particle losses are very fast and on the lower side by the largest amplitude where the “diffusion” rate becomes immeasurable.

Despite these refinements to the experiment our efforts to get quantitative results did not meet with full success. Nevertheless, some relevant intermediate results were obtained. The natural ripple spectrum was measured [3] to be $\Delta Q_x = \pm 1 \times 10^{-4}$ of which one half can be attributed to seven ripple lines between 50 Hz and 1000 Hz. One successful measurement is shown in Fig. 3: after having reproduced the detuning curve with amplitude it was possible to use octupoles of the SPS to reduce the detuning by roughly a factor of ten. Even more important is the improvement of the dynamic aperture by some 30% obtained as a result, which makes us confident that the detuning correction in the LHC will lead to some improvement as well. Tracking studies were performed up to 2.6×10^7 turns which represents 10 min of SPS storage time. It is interesting to note that a considerable reduction (10%) of the dynamic aperture still occurred after one million turns were tracked. The tracking results predicted a dynamic aperture that was 20% larger than the long-term stability border found in the experiment. However, this result was considered somewhat preliminary and we concluded that a more systematic study was needed. A general, more qualitative result of the experiment was the fact that the lifetime depended strongly on the additional tune modulation. This dependence on

tune modulation depth was also present in the tracking but did not agree quantitatively with the experiment. Moreover, in the experiment one could not confirm the frequency dependence that was expected from the tracking: the beam lifetime in the SPS seems to be rather insensitive to this parameter but very sensitive to the tune modulation depth. It has to be mentioned that the way the stability border was determined differs in the tracking and in the experiment: in the tracking the border of the onset of chaos was used, while in the experiment the actual particle loss was taken. To test the importance of this difference a toy model (a simple FODO cell plus a sextupole) was tracked for many millions of turns (see Fig. 4) with and without tune modulation. One found that the difference between cases with tune modulation on or off becomes apparent after some 10^5 turns, while the onset of chaotic motion shows up after only 20 000 turns. The more pronounced effect of the smaller tune modulation frequencies is only visible after more than 10^7 turns. This has two consequences: firstly it could very well be that the difference of the effect of the tune modulation frequencies is only visible after a very long time in the experiment (may be even after the storage time of interest) and secondly, in the case with tune modulation, the onset of chaotic motion is generally much too pessimistic as a criterion for the dynamic aperture which in our case is always the amplitude below which the motion is stable for a *given time interval*.

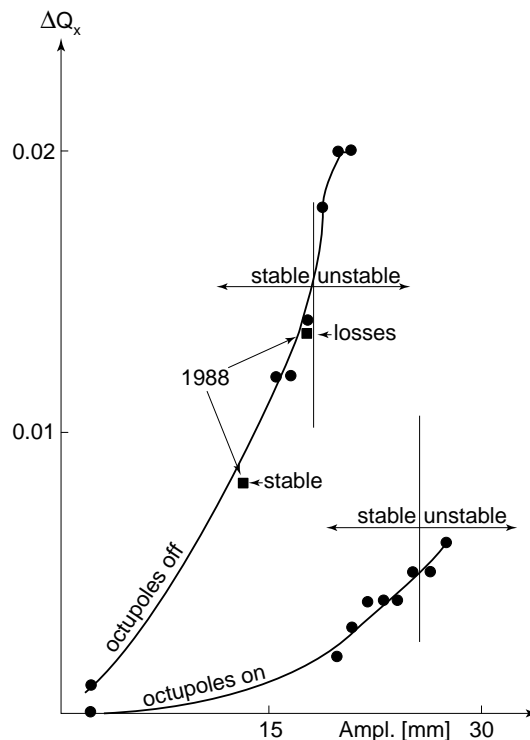


Figure 3: Detuning and stability.

An interesting side issue was the study of the effect of two simultaneous tune modulation frequencies compared with only one frequency while keeping the total tune modulation depth equal in both cases. The two tune modulation frequencies (see Fig. 5) reduced the lifetime by more than a factor of three compared with the one-frequency case. These findings led to a study which treated the case with more than one frequency in a more rigorous theoretical framework [19]. It has to be mentioned that this phenomenon may not be generally applicable but may depend on the particular parameters chosen in the SPS (see

below). Another feature often found in the experiment is the appearance of the so-called “shoulder”: right after a retraction of the scraper the intensity stays almost constant (infinite lifetime), and after a certain time interval, the intensity bends over rather abruptly without a smooth transition leading to a constant finite lifetime. This phenomenon was studied in Ref. [16] and found to be in contradiction with a simple diffusion mechanism. Finally we would like to mention a related study concerning slow particle losses in hadron colliders [20] which gives a phenomenological description of these losses in phase space.

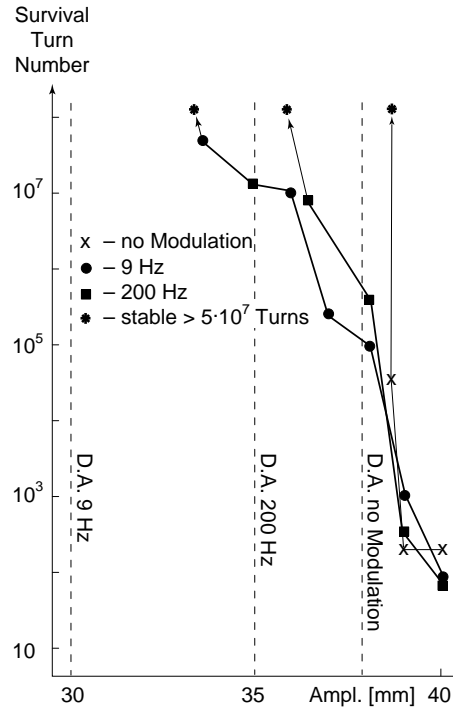


Figure 4: Long-term stability with tune modulation.

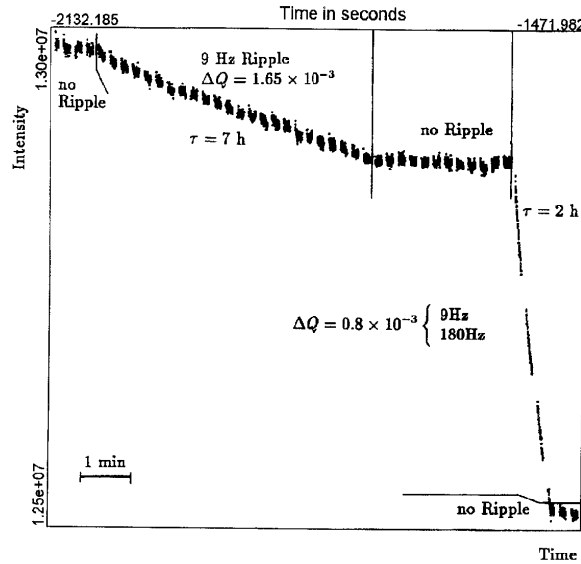


Figure 5: One and two tune-modulation frequencies.

In this section we describe the instrumentation for the dynamic aperture experiment at the SPS. In particular our main instruments, the data acquisition system BOSC (the acronym stands for Beam OSCillations) and the wire scanner system, are covered in detail. The experimental conditions are presented in the next subsection. Then we describe the tracking model for the SPS and explain in detail all methods used in our tracking simulations. In the last subsection we show that our model reproduces the basic nonlinear behavior of the SPS. This is absolutely mandatory in order to proceed with the long-term studies. Furthermore it was also necessary to carefully calibrate our instruments.

3.1 Instrumentation for the SPS experiment

The CERN SPS used for the experiment is a synchrotron with 1100 m mean radius. It can accelerate protons from 14 GeV up to 450 GeV for fixed-target experiments. In the following we describe the general instrumentation (see Fig. 6) needed for this experiment.

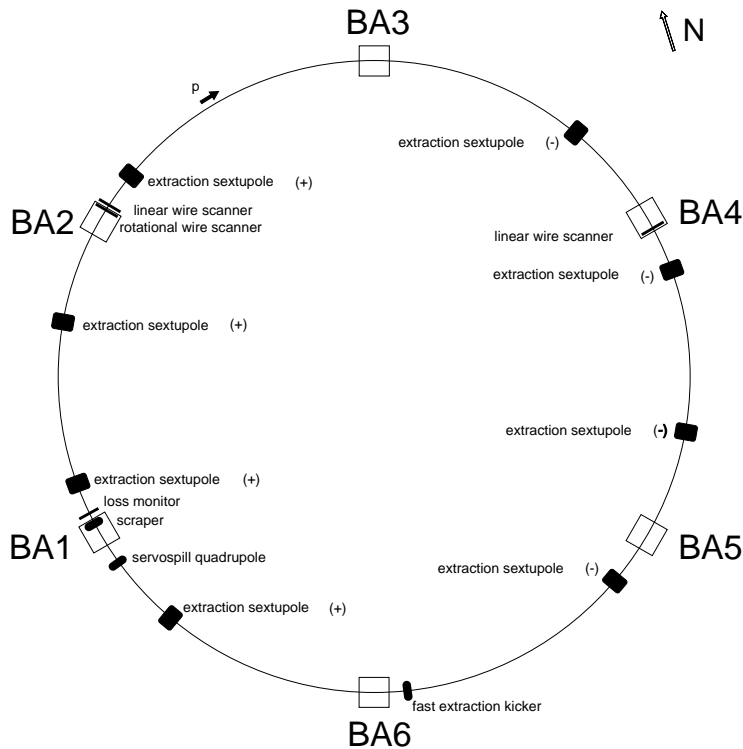


Figure 6: Instrumentation at the SPS. The eight strong sextupoles, the servospill quadrupole (the source of additional tune modulation), and the kicker magnet are shown at their locations in the SPS. The positions of the linear and rotational wire scanners, the scrapers, and the loss monitor are also given. (BA stands for access hall.)

Sizable nonlinearities are introduced by eight sextupoles (part of the slow extraction system) which are about 10 times stronger than the chromaticity sextupoles located at the focusing quadrupoles. They are grouped in two families with different polarity (Fig. 6) so as to avoid a change of the chromaticity and the excitation of the third-order resonances. Analytical calculations predict that these strong sextupoles lead to a detuning with action 10 times larger than in the normal machine.

A single quadrupole (BA1 in Fig. 6) is used to introduce additional tune modulation. This quadrupole operates linearly up to a modulation depth of $\Delta Q_x = \pm 1.5 \times 10^{-3}$ which

is more than tentimes the natural one. In the frequency range up to about 200 Hz the response of the magnet to the signal input is linear as well.

A kicker magnet (BA6 in Fig. 6) has been used to vary the average amplitude of the particle beam. It has been calibrated several times (see Fig. 7) and shows a very linear behavior down to small kick amplitudes. Whereas the measurement of 1993 showed a degradation in the kick strength of 10% compared with earlier measurements, the calibration of 1995 showed practically no difference from the measurement of 1993.

Pairs of horizontal and vertical scrapers (BA1 in Fig. 6) served as aperture limiters and the losses at these scrapers were detected by a scintillator placed close by (45 m downstream). Scraper positions and the loss detector signal were recorded by the BOSC system (Sec. 3.1.1).

Momentum and tune distributions were measured with a Schottky system [21]. Using the same hardware, a continuous tune measurement system was set up to measure the natural tune ripple spectrum (Fig. 8).

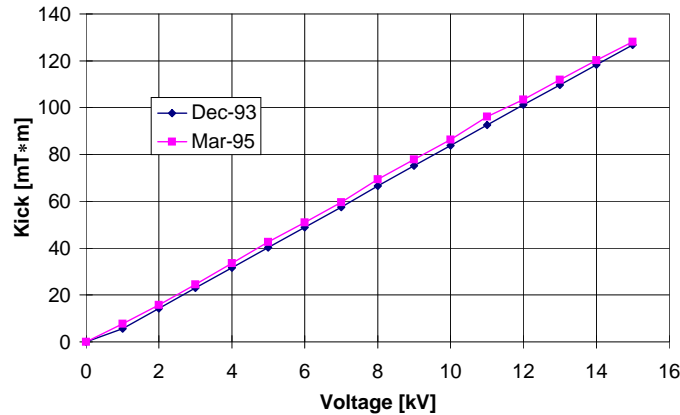


Figure 7: Calibration of the kicker in 1993 and 1995.

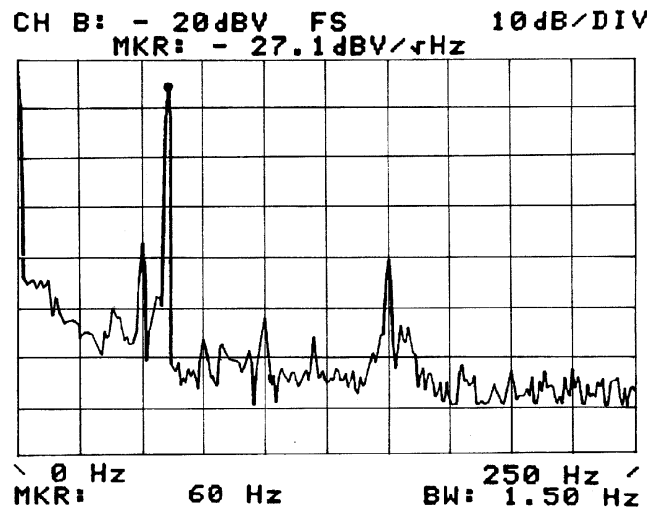


Figure 8: Natural tune ripple spectrum. Up to 250 Hz, three natural tune ripple lines are above the noise level (50, 100 and 150 Hz) as expected from the voltage power supply ripple. The large 60 Hz line has been introduced by our modulated quadrupole and is used for calibration purposes.

The turn-by-turn beam data acquisition system and the flying wire system which are most relevant for our experiment will now be described in some detail.

3.1.1 Data acquisition system BOSC

The turn-by-turn data acquisition system BOSC [22] was originally intended to be used in the SPS to measure the intensity and the position of the individual proton and antiproton bunches over a full machine cycle. Now a wide range of different signals can be recorded. The system consists of a VME crate with a 68030 CPU card, a timing module, a bunch selector card, and 12 ADC cards each with two channels to acquire and store the data from up to one million turns. Three such crates on the SPS site and one crate on the LEP site can be addressed by Apollo or HP-UX workstations via Ethernet and Token Ring. Very flexible measurement requests can be sent to the crates in data structures which are then filled with the requested data and sent back to the workstation for processing. In the crate a complex control software running under OS9 has been developed, with several application software programs now running either on Apollo or on HP-UX workstations under Xwindows/MOTIF. Apart from its use in the SPS dynamic aperture experiment, with its constantly changing requirements, BOSC also provides the operational tune measurement in the SPS.

a. Hardware description

The BOSC acquisition system in its final form is housed in a VME crate. It can handle up to 24 analog signals which are taken from homodyne receivers. They are organized in 12 dual-channel electronic cards (*dual sampler*) which contain 1 MByte memory for each channel to allow the measurement turn by turn over a period of more than 20 s in the SPS. The acquisition bandwidth of 5 MHz is well matched to the bandwidth of the receivers. A logic cell array common to both channels on the ADC card acts as a slave to the crate CPU. The system is mainly intended for the measurement of single bunches. The *bunch selector* picks a given bunch circulating in the machine. The time resolution of this selection is determined by the bandwidth of the system and is at present of the order of 200 ns. Special care has been taken to isolate the low-power analog circuits from the high-power digital circuitry. The connection between the two is made in the *VME bridge* module. The information concerning the machine cycle-time is fed into the system by a timing module.

At present three units are installed in the SPS and one in LEP:

- A first one is dedicated to turn-by-turn position measurements. It is used to derive the machine tunes. A number of channels are connected to 200 MHz receivers. They are well adapted to measure single lepton bunches. However, they are also used to measure the SPS proton beams bunched at 200 MHz. Special low-frequency FET amplifiers with a bandwidth reduced to 5 MHz to match the acquisition system are connected to a second set of channels. They allow the measurement of bunched and unbunched beams. The excitor for this measurement can either be a special fast kicker magnet or the deflector plates of the transverse feedback system. The excitation of the latter is controlled by BOSC using the *sequencer* unit.
- A second BOSC unit is devoted to single-bunch intensity measurements. The signals are generated by 20 MHz homodyne receivers.
- A third unit acquires much slower signals generated by DC current transformers, collimator movements, and scintillators.
- The LEP unit records the intensity and beam-position signals of one beam-position monitor for one bunch of electrons and positrons, respectively.

The control software [23], running under OS9 on the 68030 processor, has the following tasks: setting up the communication between the crate and the workstation, setting and changing some hardware parameters, taking measurement requests from a workstation, starting the data acquisition on the crate, and sending the data to the workstation after an acquisition has been made. It is capable of handling several requests simultaneously on the same crate.

The communication is done over Ethernet and Token Ring where sockets under TCP/IP are used. For the data transfer in any direction MOPS data structures are used [24]. A schematic overview of the system consisting of the crate, the workstation, and the communication part is given in Fig. 9.

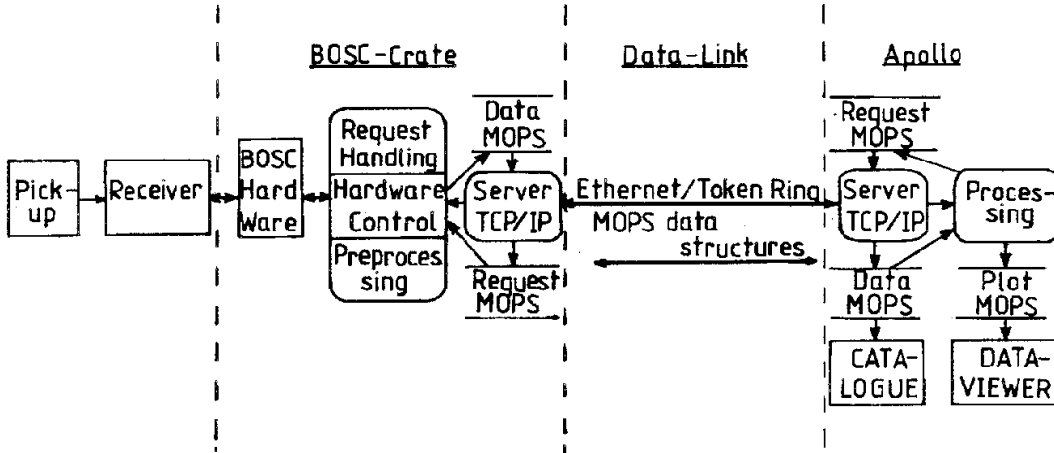


Figure 9: Setup of BOSC.

It is possible to change some of the parameters controlling the hardware such as base addresses, gains, and bunch selector settings. The use of base addresses allows the translation from physical to logical channel addresses, so as to freely choose channels without the need to swap cables. The receiver gain can be changed from 14 dB to 70 dB in 14 dB steps, each ADC channel gain can be changed from 0 dB to 24 dB in 6 dB steps.

The MOPS data structure that is sent to start the measurement on the crate in one of its objects holds a coded request (nine integer numbers) that specifies the measurement parameters: on which BOSC crate to run the measurement, the number of super cycles to be measured, the start time of the measurement in the SPS super cycle, the time between blocks of acquisitions, the number of acquisition blocks, the time between sub-blocks of acquisitions, the number of sub-blocks in one block, the number of turns per sub-block, and the channels to be used for the measurement. An example of the use of some of these parameters can be found in Fig. 10. A server program runs on both ends to receive MOPS data structures with measurement requests or acquired data, respectively. The data read from the ADC memory and hardware settings, such as timing information, are added to the request MOPS data structure that has been sent from the driving workstation.

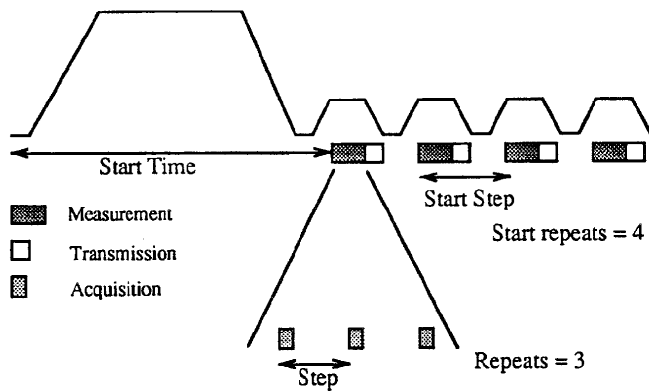


Figure 10: Time structure of a BOSC measurement [23].

c. Application software description

The application software [23] is an interface for starting a measurement, displaying the data acquired, storing data, and performing a detailed postprocessing analysis. For displaying data the *dataviewer* program is used [25], the archiving is managed by a catalog package [24]. BOSC is now used as an operational tool for tune measurement [26] as well as a tool for the dynamic aperture experiments performed on the SPS. In the following we only report on the latter application software package. There are two main types of measurements that can be performed:

- Lifetime measurements
- Phase space measurements

In the dynamic aperture experiments we want to investigate effects that influence particle stability over long periods. It is therefore very convenient to use BOSC for simultaneous and continuous beam-intensity, scraper-position, and loss-monitor readings. Different phenomena leading to particle loss can thereby be easily distinguished (see Fig. 11).

For a phase space measurement the position and intensity signals of one or more pickups can be recorded. After having applied a kick to the beam, the Fast Fourier Transforms from the position signals give the tunes and the line spectra due to resonances. Figure 12 shows how readings of two pickups separated by a multiple of 90 degrees allow the depiction of phase space projections. Currently we take and analyze online two samples of up to 65 000 turns, the repetition rate being 30 s. This allows a very precise determination of the tune, but also linear coupling correction, chromaticity compensation, and identification of high-order resonances.

For phase space measurements there is a tool box which contains four programs. The *fft_mod* program allows one to compute the spectra for a selected range of turns. With this facility one can detect changes in the tunes, for instance due to power supply ripple. The *stroboscope* program plots only every n th point in phase space thereby visualizing resonances in the horizontal, vertical, and physical phase space projection. The *fake* program has the same functionality as *stroboscope* but uses the information of only one pickup by plotting an x -coordinate at turn number i versus the x -coordinate at turn number $i + \text{skip_step}$. The *smear* program computes the horizontal and vertical decoherence, the decoherence-corrected amplitude, and the “smear” [27].

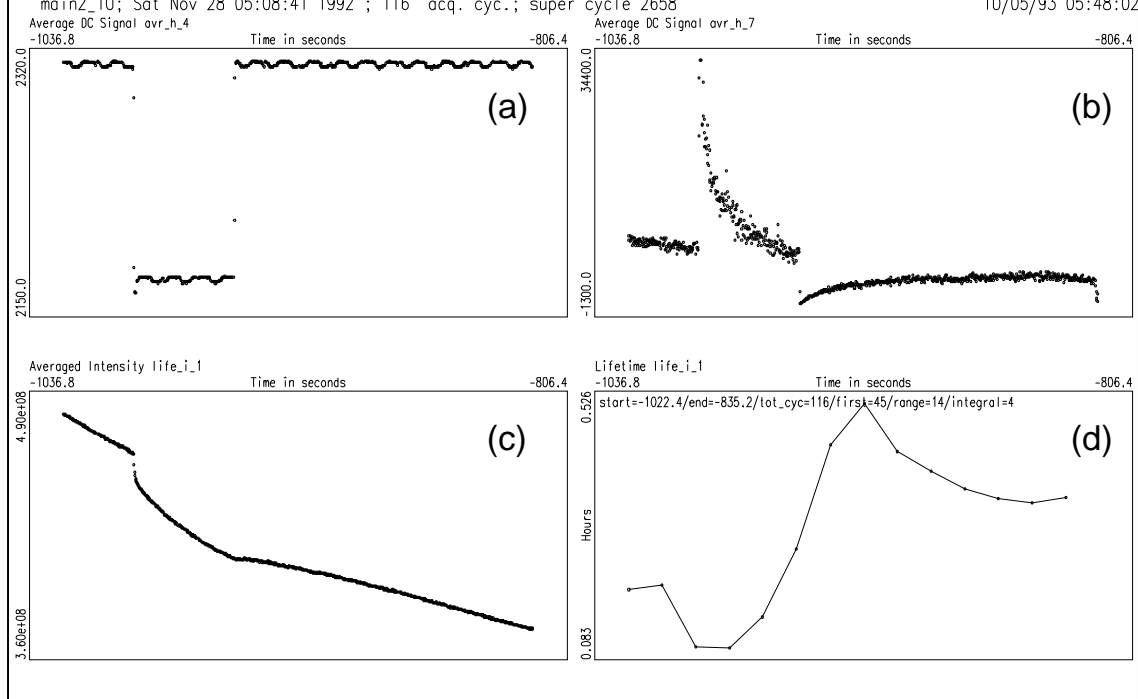


Figure 11: Lifetime measurement. The effect of moving a scraper (a) can be seen on the loss monitor (b), the beam intensity (c), and the lifetime (d).

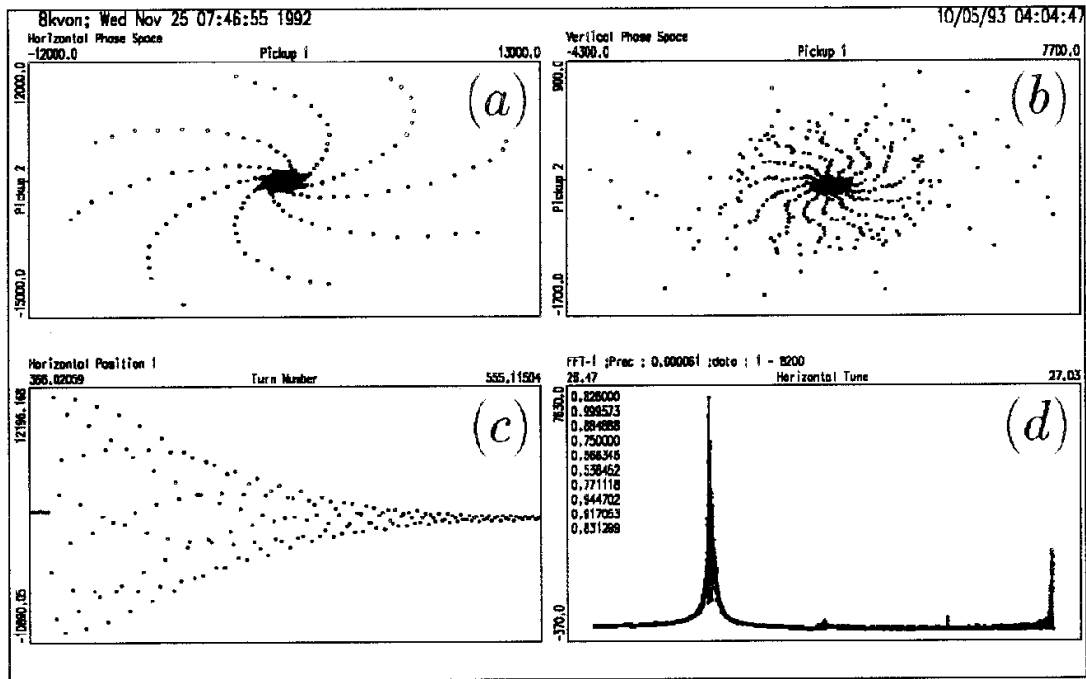


Figure 12: Phase space measurement. Motion is depicted close to a horizontal 8th order resonance (a), on (b) the vertical phase space plot is shown. The horizontally kicked and decohered beam can be seen on (c) and the horizontal FFT on (d).

Since 1984 rapid wire scanners have been used in the SPS to measure the transverse emittances [28]. A carbon wire of $36\ \mu\text{m}$ thickness, fixed in a turnable fork (“rotational” scanner), went through the beam with a speed of about 6 m/s. These scanners are still in operation (see BA2 Fig. 6).

Later on two “linear” wire scanner units were installed (in BA2 and BA4, see Fig. 6) to improve the quality of the measurements. In these scanners the wire is fixed in a shiftable fork (Fig. 13), moving at a speed of 0.4 m/s. Secondary-particle emission caused by the beam hitting the wire can be observed using either scintillators or the depletion current in the wire itself.

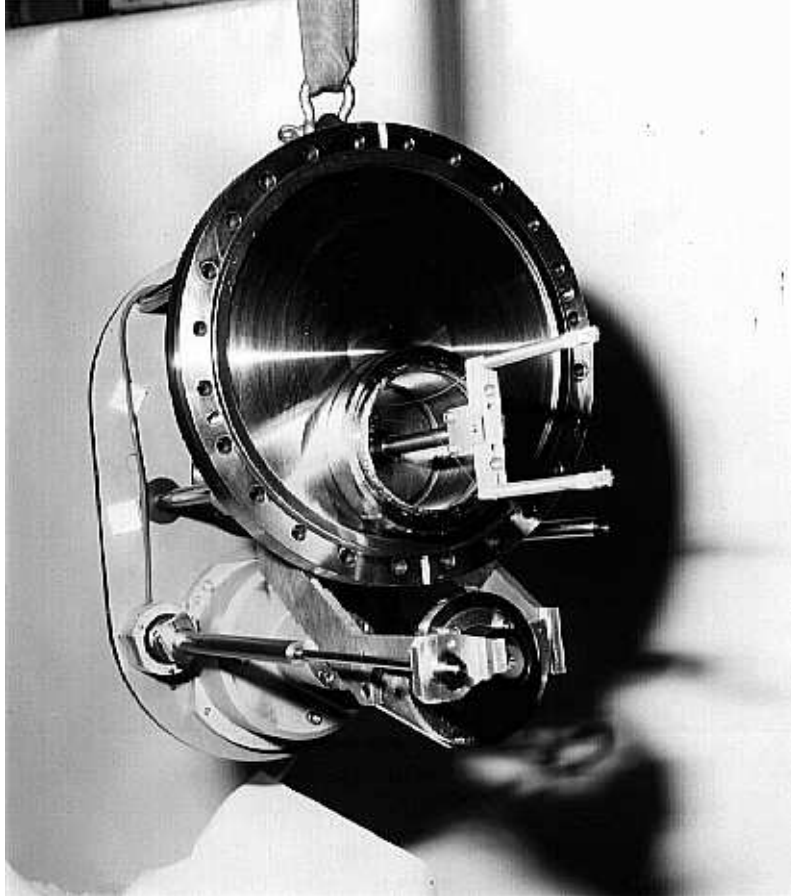


Figure 13: Hardware to support the wire.

An application software package [29], running on workstations in the control system, allows one to trigger the scanner, to set gains (voltage for the photomultiplier or amplification for the depletion current), to choose the timing in the SPS supercycle, to display the scans together with their fitted Gaussian curves, and to archive the data. To store the large amount of data produced in the dynamic aperture experiments an extended catalog has been created. In Fig. 14 the wire scanner functionality is shown in a block diagram.

After the beam has been kicked a typical double-peak structure appears in the signal (Fig. 15). To test the impact of the wire on the beam under these circumstances many scans have been performed. For the original $36\ \mu\text{m}$ -thick wires a drop in the intensity could be observed for each scan [Fig. 16 (a)]. The loss per scan could be estimated to be

2.9×10^{-6} of the total intensity. The subtle effects we wanted to study in this experiment are of the same order of magnitude as the effect of the thick wire. Therefore, it was decided to replace the $36 \mu\text{m}$ carbon wires in BA4 with $8 \mu\text{m}$ wires (Fig. 17) for both the horizontal and vertical scanner, respectively. With such a thin wire the intensity loss per scan was reduced to some 0.7×10^{-4} per scan [Fig. 16 (b)] and no beam blowup could be observed. With the position resolution of the ruler and the sensitivity of the scintillator, 5×10^7 protons (10^{-4} of a typical intensity) can be clearly detected at the edge of the beam profile.

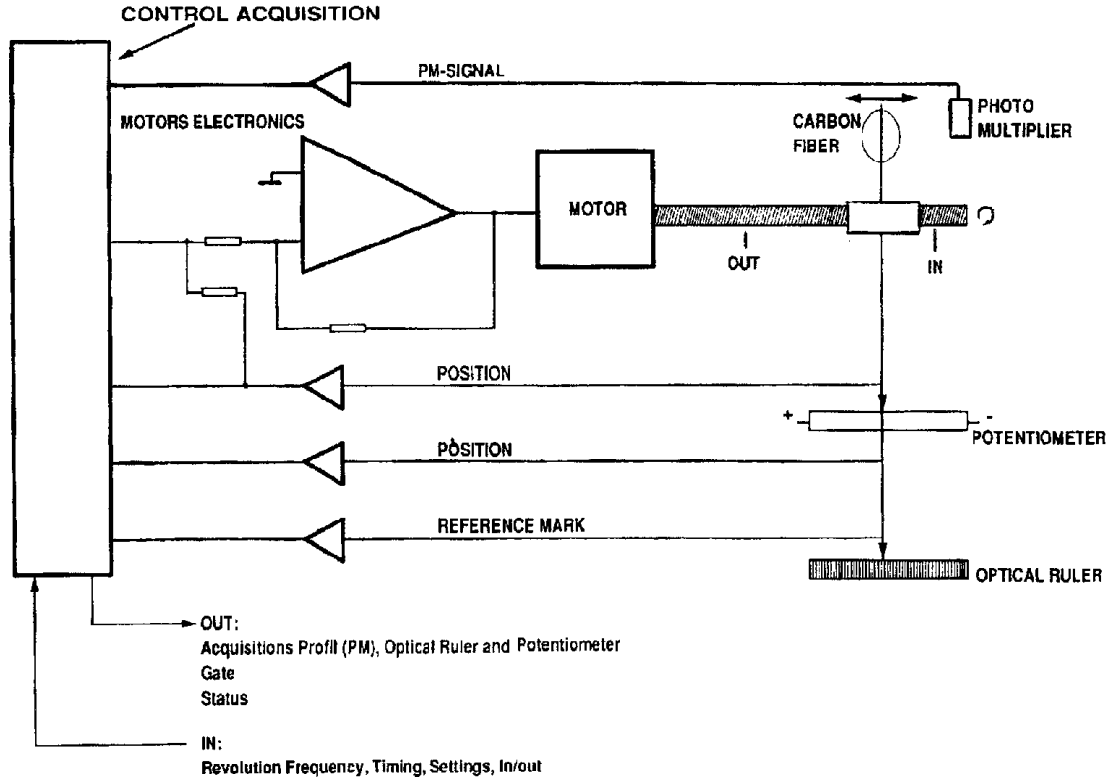


Figure 14: Wire scanner system block diagram.

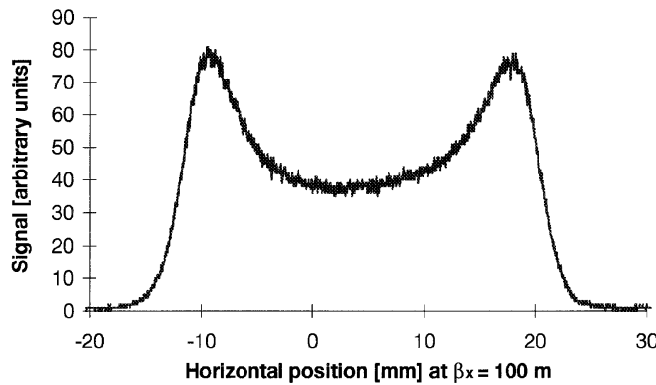


Figure 15: Example of a wire scan of the kicked beam.

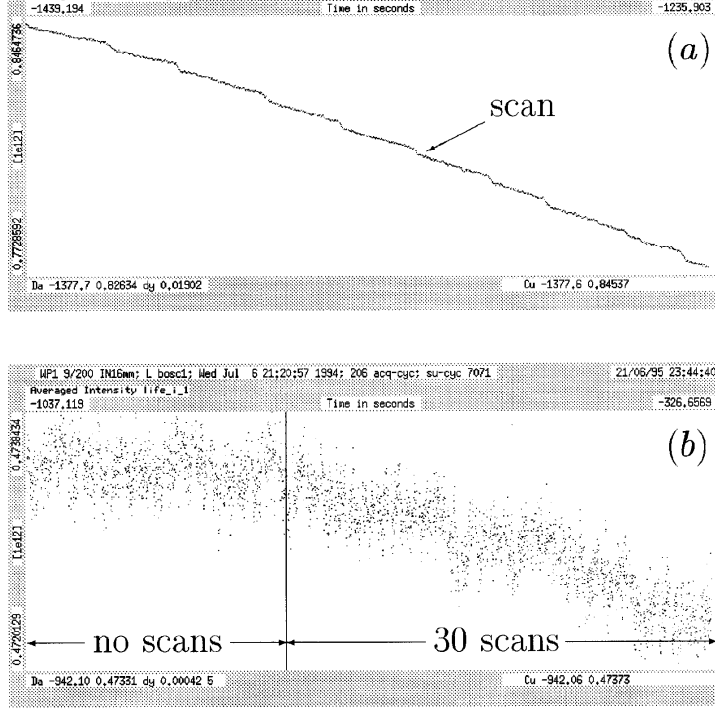


Figure 16: Influence of wire scans on beam intensity.

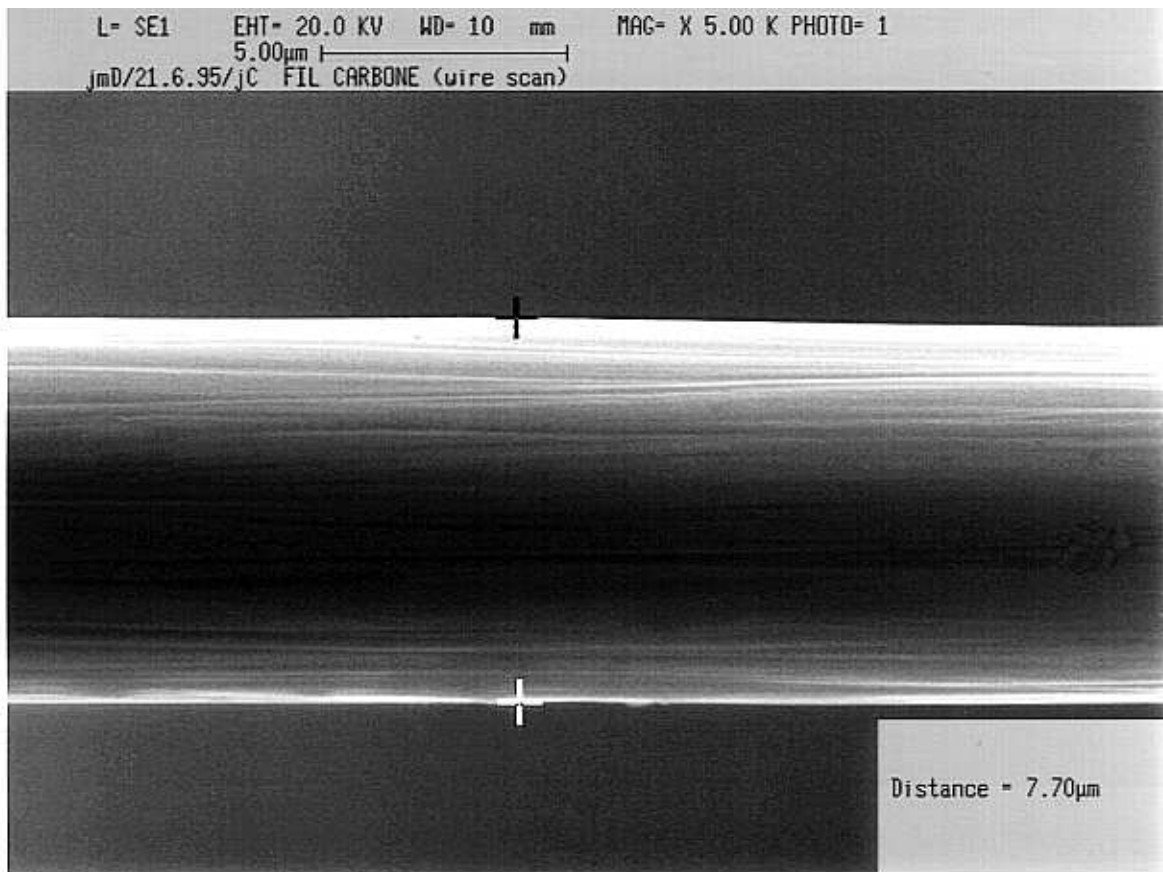


Figure 17: Microscopic view of the thin carbon wire ($8 \mu\text{m}$ thickness).

3.2 Experimental conditions

The energy of 120 GeV was chosen in order to have small remanent fields, hardly any saturation, and negligible space charge effects, and at the same time a high efficiency of the nonlinear fields. The 1σ normalized emittance as given by the preaccelerator chain amounts to some 5 mm mrad in the horizontal and vertical plane. The intensity was kept below 10^{12} protons to minimize the resistive-wall effect [30]. The momentum spread was measured with the longitudinal Schottky signal to be some 10^{-3} . In each experimental session the closed orbit, the linear coupling, and the chromaticity were corrected to very high precision. The detuning curve was measured and the short-term dynamic aperture evaluated.

This preparation was done in pulsed mode. Every 14.4 s the proton beam was injected into the SPS, accelerated to 120 GeV, and kept at this energy for 8 s while we carried out our studies. Once the strong sextupoles were turned on, all systems normally used to counteract collective instabilities could be switched off and the kicker was used to explore different amplitudes.

The long-term studies were performed in a continuous mode with the RF switched off (coasting beam) since RF noise could not be reduced to acceptable levels. With the continuous-tune measurement system [21] the natural ripple spectrum showed seven major lines that add up to a total modulation depth of 0.5×10^{-4} , which is half the measured total tune ripple depth. All these conditions are summarized in Table 1.

Table 1: Fixed beam parameters for the SPS experiment

Energy E	120 GeV
1σ normalized emittance	≈ 5 mm · mrad hor. and ver.
Intensity I (beam current)	$< 10^{12}$ p (7 mA)
RF	short-term on, long-term off
Momentum spread $\Delta p/p$	$\approx 10^{-3}$
Closed-orbit rms	≤ 0.3 mm hor. and ver.
Linear coupling	$ Q_x - Q_z \leq 0.003$
Chromaticity $Q' = \Delta Q/(\Delta p/p)$	≈ 1 hor. and ver.
Natural tune ripple lines	50, 100, 150, 300, 350, 500, 600 Hz sum of modulation depth $0.5 \cdot 10^{-4}$
Total natural tune ripple depth	1.1×10^{-4}

In Table 2 the studied parameter range of the experiment is shown. The two working points WP1 and WP2 are depicted in Fig. 18 together with the detuning due to the nonlinearities (see Sec. 3.4). WP1 is close to a horizontal 8th order resonance, WP2 is close to a horizontal 5th order resonance. Both resonances are strong but do not define the dynamic aperture. However, a number of 7th order resonances lead at both working points to particle loss.

The additional modulation frequencies (9, 40 and 180 Hz) were chosen for the following reasons: 9 Hz to test the low-frequency range, 40 Hz as a frequency close to but different from the main power supply ripple frequency of 50 Hz, and 180 Hz as a typical synchrotron frequency. Experiments were also made with combinations of two frequencies. The horizontal tune modulation depth was 0.5×10^{-3} , 1.1×10^{-3} and 1.87×10^{-3} , the larger values being applied at WP1 to obtain loss rates similar to those at WP2. The

ratio of horizontal and vertical tune modulation depth was $\Delta Q_x/\Delta Q_z = 1.75$ given by the beta functions at the ripple quadrupole.

The kick strength was varied to probe different amplitudes up to the dynamic aperture. Furthermore, the scrapers were used to precisely define the edge of the beam.

Table 2: Studied parameter range for the SPS experiment

Working points (Q_x, Q_z)	WP1 (26.637, 26.533) WP2 (26.605, 26.538) others
Tune modulation frequencies	9, 40, 180, 9+40, 9+180 Hz
Horizontal tune modulation depth	0.5×10^{-3} , 1.1×10^{-3} , 1.87×10^{-3}
Kick strength (at $\beta_x = 100$ m)	1.9–19.5 mm
Horizontal scraper position	from 10.8 mm to the beam pipe

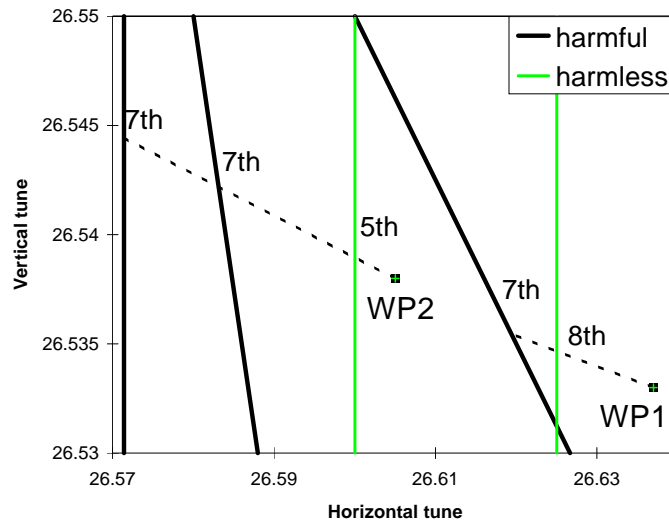


Figure 18: The working points WP1 and WP2 in the tune diagram.

3.3 Tracking model and methods

The computer code SIXTRACK [31] was used for the tracking studies. Drifts, dipoles, and quadrupoles were modeled as thick lenses; all other elements, skew quadrupoles and sextupoles, were approximated as thin lenses. Apart from the eight strong sextupoles, the 108 chromaticity correction sextupoles were included in the model. The effect of the closed orbit was introduced by shifting the sextupoles by the measured values, the linear coupling was adjusted to the measured one using one family of six skew quadrupoles, and the chromaticity was corrected to zero. Particles were distributed in amplitude and momentum to probe a sufficient fraction of the phase space. The scraper was used as observation point because the losses were detected at that place in the experiment.

One of the tools [32] to analyze and understand phenomenologically the intricate nature of particle motion in phase space is an elaborate postprocessing of the tracking data. The methods applied are listed below.

Tune: The tune was determined for each case and amplitude with the FFT and the averaged phase advance per turn.

Smear: The phase-dependent distortions of the linear invariants in phase space due to the nonlinearities can be evaluated with the “smear”, a concept described in Ref. [27]. It is needed as a complement to the dynamic aperture which is usually stated as one amplitude only. Moreover, strong but stabilized resonances produce a peak in the smear-versus-amplitude plot.

Chaos: The time evolution of the distance of initially close-by particles allows one to distinguish between regular and chaotic motion. Chaotic motion manifests itself in an exponential growth of this distance which grows linearly for regular motion.

Survival plots: The loss time versus amplitude (denoted as survival plot, see Ref. [33]) was our main tool for determining the dynamic aperture in the simulations. Typically the loss time increases exponentially with decreasing amplitude, and very close to the regular region it tends to infinity.

Averaging: When tune modulation was switched on, the phase advance was averaged over one tune-modulation period to derive meaningful numbers for the tunes. The particle amplitudes were averaged as well over that period to study their mean and rms values as a function of time.

All simulation studies were performed on an IBM RISC station cluster [34]. For one turn in the SPS (0.023 ms real time) a computing time of about 1.5 ms per particle pair was achieved on this system when using the vectorized code. This means that for a typical long-term run with 32 particle pairs and the maximum turn number of 26 million turns (equivalent to 10 min storage time) a CPU time of roughly two weeks is needed.

3.4 Preparatory measurements

In this section we describe the calibration of the instrumentation needed for the experiment. Moreover, a detailed comparison is given of the amplitude-dependent tunes from experiment and tracking.

3.4.1 Calibration measurements

For the long-term stability measurements it was mandatory to calibrate the instrumentation to achieve the necessary precision. All wire scanners (both linear and rotational) were calibrated against each other and agree within some 5–10% which also increases our confidence in the knowledge of the beta functions around the ring.

More important was the exact knowledge of the kicker-magnet strength as this defines the mean amplitude of the particle distribution. Besides the test of linearity (see Sec. 3.1), the absolute calibration was done using the wire scans of kicked beams and measuring the distance of the two peaks [35]. The initial approach to use scrapers for the calibration had to be discarded for various reasons (imprecision of scraper position, closed-orbit and particle distribution uncertainties).

3.4.2 Detuning with amplitude

Since the amplitude-dependent tune is an important property of any nonlinear oscillator system, even a modest disagreement between tracking and experiment would cast doubt on the validity of the tracking model.

Particle motion in hadron accelerators can be described in the Hamiltonian formalism [36]. Transforming the usual accelerator coordinates into action–angle variables so

that the phase-dependent part of the Hamiltonian can be neglected, the lowest order part of the nonlinear Hamiltonian can be written as

$$H = aI_x^2 + 2bI_xI_z + cI_z^2 \quad (1)$$

where I_x and I_z are the horizontal and vertical action, respectively, and a , b , and c the so-called detuning coefficients. The action variables are related to the Courant–Snyder variables by [37]

$$2I_{x,z} = \frac{1}{2\pi} \int_0^{2\pi} d\phi_{x,z} \epsilon_{x,z}(\phi_{x,z}, \phi_{z,x} = \text{const}). \quad (2)$$

The detuning can therefore be expressed as

$$\Delta Q_x = 2aI_x + 2bI_z, \quad (3)$$

$$\Delta Q_z = 2bI_x + 2cI_z. \quad (4)$$

In our case, where sextupoles are the dominant nonlinear elements, Eqs. (3) and (4) can be derived in second-order perturbation theory.

In Figs. 19 and 20 the detuning as a function of action is depicted for the model and the experimental data, respectively. As expected from Eqs. (3) and (4) the increase of the detuning is linear with action. The extensive experimental data agree very well with the expectation from the model, in the horizontal as well as in the vertical plane. Table 3 summarizes all detuning coefficients, where a and b are taken from the experiment and the model, while the term c was not measured since we concentrated our studies on the horizontal plane only.

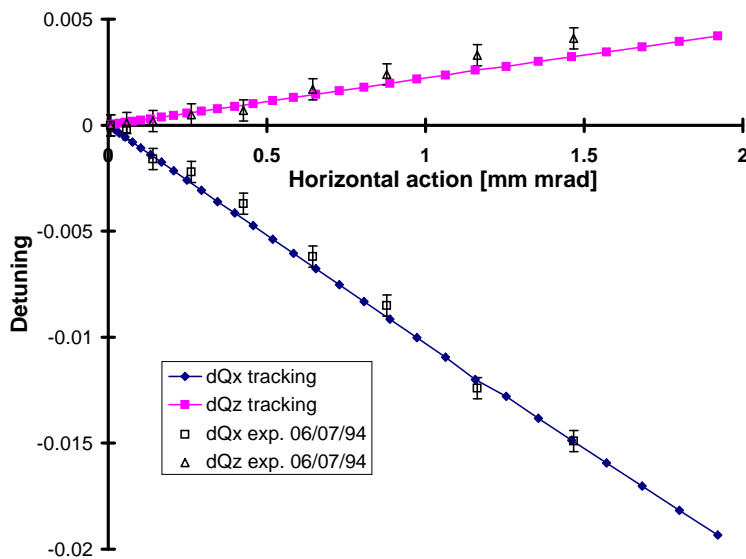


Figure 19: Detuning as a function of action at WP1.

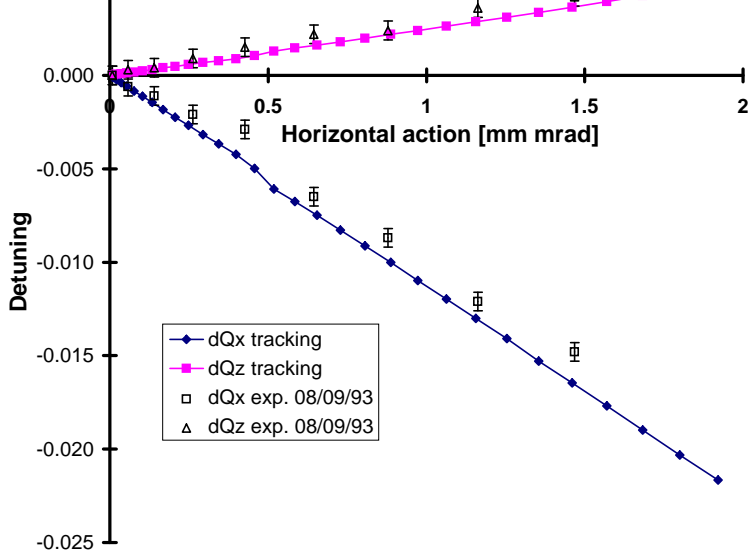


Figure 20: Detuning as a function of action at WP2.

Table 3: Detuning coefficients at WP1 and WP2

	a [$10^{-3} (\text{mm mrad})^{-1}$]	b [$10^{-3} (\text{mm mrad})^{-1}$]	c [$10^{-3} (\text{mm mrad})^{-1}$]
WP1	-5.2	1.1	-0.3
WP2	-5.6	1.2	-0.3

4 THE SCRAPER EXPERIMENT

The detection of slow particle losses in the experiments of 1989 was the starting point for an extensive series of experiments to study particle losses as a function of betatron amplitude, modulation depth and frequency. Emphasis was put on obtaining quantitative results. We were faced, however, with the problem that the particle distribution extended over a wide range of amplitudes rather than a narrow one.

To partially overcome this problem, the experiment was performed in the following way: firstly, a single kick of well-defined strength was applied instead of blowing up the beam with many small kicks. Although the latter choice had considerable operational advantages for our purposes, we chose the first alternative because the maximum of the particle distribution was thereby placed at the desired amplitude and the resulting distribution could be estimated analytically (see Appendix A in Ref. [35]). Secondly, a scraper was used to define a maximum betatron amplitude and, after a subsequent retraction, it acted as the physical aperture. Thirdly, for reasons of reproducibility, a complex experimental procedure had to be strictly followed (cf. Fig. 21): first the horizontally kicked beam was scraped vertically to remove the vertical beam tail (time T_{-3} , intensity I_{-3}). Then the vertical scraper was retracted, the horizontal scraper was moved in (T_{-2}, I_{-2}) , and the additional tune modulation was switched on (T_{-1}, I_{-1}) . After waiting until a stationary particle distribution with an approximately constant loss rate was produced, the horizontal scraper was retracted (T_0, I_0) , typically by 1 mm, to create an amplitude region free of particles that was expected to be filled by some transport process. We expected

the losses to stabilize after a time which is denoted by T_{1b} leading to a new stationary particle distribution. We determined T_{1a} from the point of intersection of the linear slope of the intensity with the line $I_0 = \text{const}$. After some 15 min the tune modulation was switched off and the beam was scraped once more vertically (T_2, I_2) and horizontally (T_3, I_3) to determine the plane in which the particle losses predominantly took place.

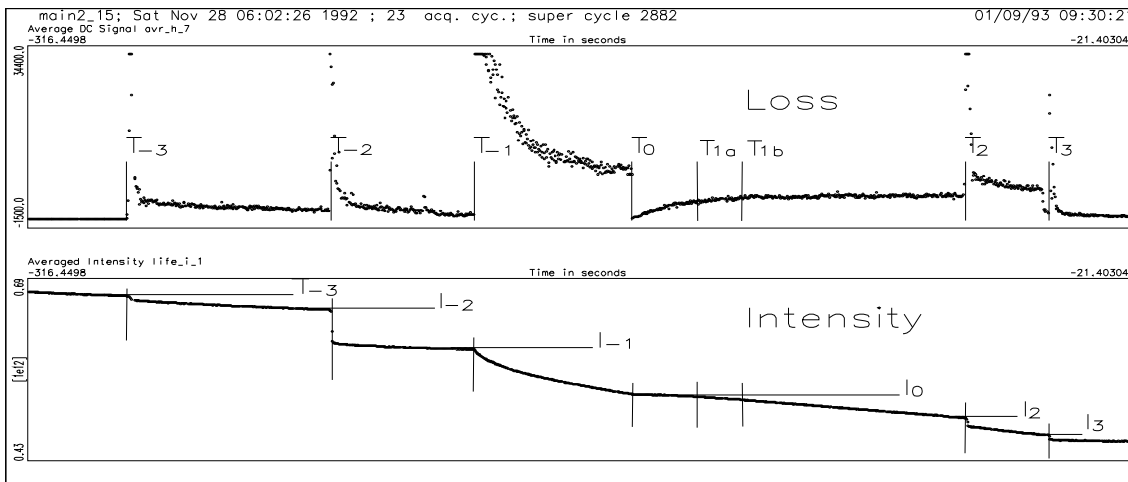


Figure 21: Loss rate and beam intensity as a function of time in the scraper experiment.

In the initial setup with heated beams as depicted in Fig. 2 the time evolution of the intensity suggested that the loss process could be described by a diffusion model. Considering the amplitude dependence of the losses the appropriate diffusion equation reads

$$\frac{\partial f(I_x, t)}{\partial t} = \frac{\partial}{\partial I_x} \left(D(I_x) \frac{\partial f(I_x, t)}{\partial I_x} \right) \quad (5)$$

with an action-dependent diffusion coefficient $D(I_x)$. Such a diffusion model was successfully applied [38] in a similar experiment with scrapers at the HERA proton ring under collision conditions, where the beam-beam interaction was the main source for the nonlinearities.

In the experimental period of 1993 that concluded this type of experiment, the following parameters were varied: At WP1 and WP2 three frequencies (9 Hz, 40 Hz and 180 Hz) and the tune modulation depths 1.1×10^{-3} and 1.87×10^{-3} were tested, in addition at WP1 the tune modulation depth $\Delta Q_x = 0.55 \times 10^{-3}$ was studied. Besides this systematic parameter scan the influence of two simultaneous modulation frequencies (9+40 Hz and 9+180 Hz) was examined at WP1 and compared with an experimental run at a different working point. A total of 61 experimental runs were recorded (a complete list can be found in Appendix B of Ref. [35]).

4.1 Experimental results

4.1.1 Intensity measurements

We will discuss results from WP2 only since in this case all tune modulation depths and frequencies were tested. In Table 4 the loss L taken 15 s after switching on the tune modulation and the time interval $T_{1a} - T_0$ is shown, which corresponds to the average transport time between the beam edge and the retracted scraper position. This time interval was the quantity originally measured in the experiment of 1989. Table 4 also holds an error if the number of cases n is larger than one.

Table 4: Experimental particle stability at WP2. The particle loss after 15 s following the switch-on time of the tune modulation is denoted by L . Time T_{1a} is determined from the point of intersection of the linear slope of the intensity with the line $I_0 = \text{const}$, n is the number of experimental runs with the same modulation frequency and depth. The given error is the $n - 1$ standard deviation of the mean value. All experimental cases were done with the same kick strength and scraper positions.

	$\Delta Q_x = 0.55 \times 10^{-3}$			$\Delta Q_x = 1.1 \times 10^{-3}$	
	L (%)	$T_{1a} - T_0$ (s)	n	L (%)	n
9 Hz	5.2 ± 1.1	13.4 ± 5.6	3	5.8 ± 3.3	7
40 Hz	6.4	13.5	1	8.9 ± 4.5	3
180 Hz	6.7 ± 2.4	17.0 ± 7.3	6	12.3 ± 6.9	4

The cases with a larger modulation depth show a larger loss L . However, the errors are so large (between 20% and 60%) that we cannot quantify reliably the difference between the different modulation depths and frequencies. The time $T_{1a} - T_0$ obtained for the smaller modulation depth has similar errors and for the larger depth it was impossible to determine even this value.

In spite of our determined efforts, these difficulties in obtaining quantitative results persisted: the beam observation tools were specially prepared and all instruments were calibrated, the linear machine properties of the SPS were measured and corrected, the nonlinear content of the machine was determined with a very good precision, and an elaborate measurement procedure was applied. The limiting parameter had been the large transverse beam size which could not be reduced below a certain limit due to operational considerations. We therefore concluded that any advances in this line of experiment would require a much smaller particle distribution in amplitude.

4.1.2 Discussion of diffusion models

Following the initial indications that the loss may be caused by a diffusion process, we were looking for a diffusion coefficient in Eq. (5) that would allow us to describe the experimental intensity curves. Any model to fit these curves had to consider a strong amplitude dependence (such as I_x^m), a maximum amplitude I_{x0} below which only a background mechanism¹⁾ D_0 leads to particle losses. We therefore arrived at a four-parameter model similar to that used in Ref. [8]:

$$D(I_x) = \begin{cases} D_0 I_x & \text{if } I_x < I_{x0} , \\ D_0 I_x + D_1 (I_x - I_{x0})^m & \text{if } I_{x0} < I_x . \end{cases} \quad (6)$$

We started with the simple approach of fitting the intensity curves at the studied amplitude to a diffusion coefficient linearly increasing with action. Of course, this requires that in the experiment the retraction distance be small compared with the amplitude studied. Unfortunately, this fitting procedure did not converge in all analyzed cases. Owing to the discouraging results obtained even for the simple case of a linear dependence of the diffusion coefficient on action, we had to refrain from a more detailed analysis using the four parameters in Eq. (6).

¹⁾ For example, rest-gas scattering leads to a diffusion coefficient $D(I_x) = D_0 I_x$ [38].

The conclusion is the same as in the previous section: the problem of the reproducibility of the experimental results due to the large transverse beam size allows neither a quantitative determination of a diffusion coefficient nor the ability to decide if such a diffusion model is appropriate to describe the loss mechanisms.

Nevertheless, we were able to obtain some interesting qualitative results concerning the so-called “shoulder”. This phenomenon, first found in 1989, can be described as follows: after the retraction of the scraper there are only small losses due to the background effect during a certain time interval. Thereafter a very linear decrease of the intensity curve over a long period without any pronounced transition region occurs (see Fig. 22). In 1993 this effect was shown to be reproducible given the same experimental conditions as in 1989. In addition in 1994 we found at WP2 several “shoulder” cases, but under different conditions than the years before. A general prerequisite seemed to be an initial scraping down to small amplitudes. This observation of a “shoulder” was shown to be in contradiction with a diffusion model [16].

Moreover, detailed tracking studies (Sec. 6) seem to indicate that a diffusion model like Eq. (6), which is valid over the whole phase phase, does not fit the phenomenology of the loss processes.

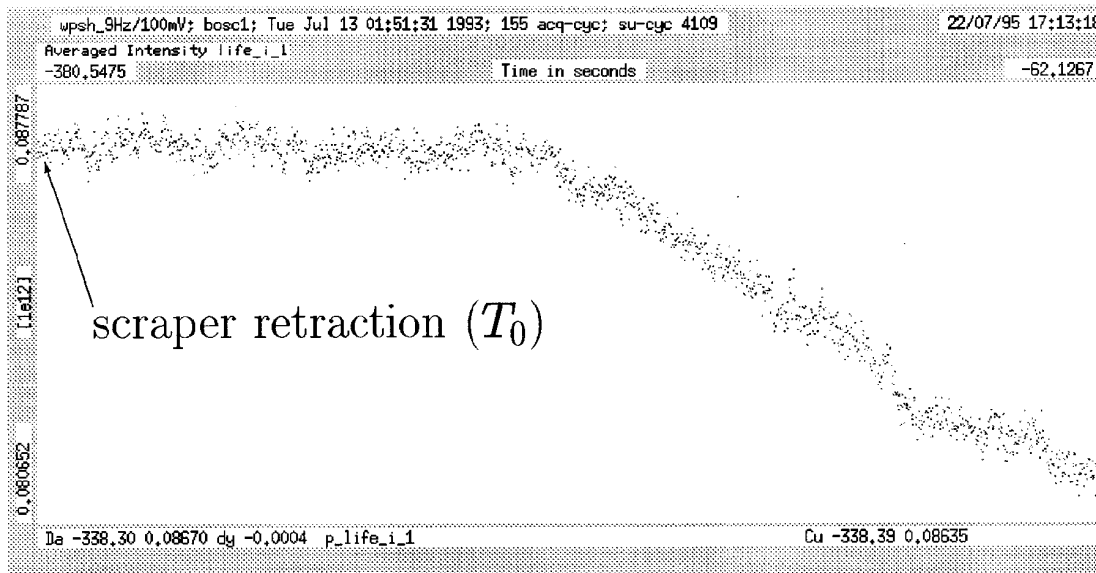


Figure 22: The “shoulder”.

4.1.3 Effect of two modulation frequencies

In 1991 an experimental case was studied in which the lifetime dropped to about one-third when two frequencies (9 Hz and 180 Hz) were applied compared with only one frequency (9 Hz), while keeping in both situations the same total tune modulation depth (Fig. 5). The same setup was tested in 1993 at another point [WP1, see Fig. 23 (a)] and for comparison the case at the original working point was repeated [Fig. 23 (b)]. For the latter case the same qualitative result could be obtained as in the previous experiment. However, in case (a) the effect of two frequencies is less pronounced than in case (b). This can be understood qualitatively as follows.

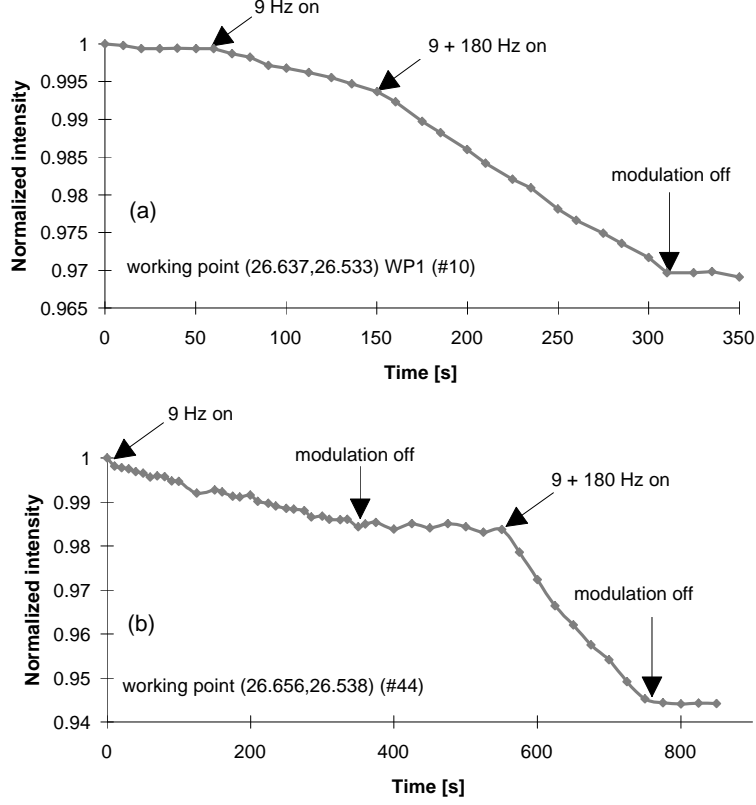


Figure 23: Comparison between one and two modulation frequencies.

With only one modulation frequency the resonance condition reads

$$kQ_x + lQ_z + m \frac{f_{\text{mod}}}{f_{\text{rev}}} = p, \quad (7)$$

f_{mod} being the modulation frequency and f_{rev} the revolution frequency, i.e. resonance sidebands are created around the main resonance $kQ_x + lQ_z = p$. For high modulation frequencies the sidebands have a large spacing; for low frequencies the spacing is small and the sidebands may overlap so that particles can be transported over wide amplitude regions. With two modulation frequencies the resonance condition is

$$kQ_x + lQ_z + m \frac{f_{\text{mod1}}}{f_{\text{rev}}} + n \frac{f_{\text{mod2}}}{f_{\text{rev}}} = p. \quad (8)$$

Having a high and a low modulation frequency (in our case $f_{\text{mod1}} = 180$ Hz and $f_{\text{mod2}} = 9$ Hz) the high frequency f_{mod1} leads to largely spaced sidebands $kQ_x + lQ_z + m (f_{\text{mod1}}/f_{\text{rev}}) = p$ around the main resonance. Around those principal sidebands additional sidebands due to the low frequency f_{mod2} are created which can overlap [19].

In Fig. 24 the working points for both cases are shown together with the detuning lines (dotted) up to the dynamic aperture. In case (a) at WP1 the dynamic aperture is close to a 7th order resonance, in case (b) it is close to a 5th order resonance. In both cases only the first-order resonance sidebands due to the higher frequency (180 Hz) are depicted which are by far the strongest sidebands for the chosen modulation depth and frequency. One of the sidebands at each working point can reach the particle distribution.

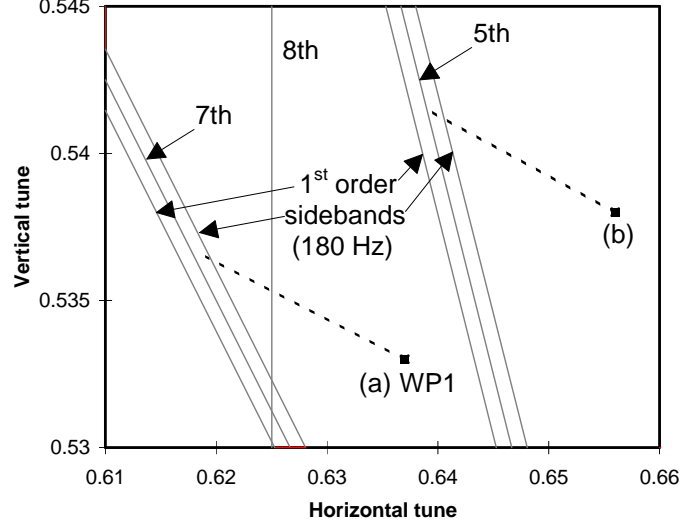


Figure 24: Tune diagram for the cases where two modulation frequencies were applied simultaneously.

From tracking data the resonance driving term of the 5th order resonance in case (b) was found to be about a factor 500 larger than the driving term of the 7th order resonance in case (a). We therefore expect that the island sizes (which are of the order of the square root of the resonance driving terms) of the resonance sidebands around the first-order 180 Hz sidebands in case (b) are much larger than those in case (a). As a consequence, more of these sidebands can overlap and the amplitude region of overlapped sidebands is larger leading to a stronger particle loss in case (b).

4.2 Intensity curves obtained from numerical simulations

In parallel with the experimental activities computer simulations were carried out. We aimed at reproducing the experimentally obtained intensity curves for the different modulation frequencies and depths. In these simulations we restricted ourselves to WP2 as sizable particle losses were found prior to 10^6 turns in the amplitude region of interest.

4.2.1 Method of reconstruction

The main problem of our experiment was to control the amplitude distribution of the particles in the beam. It was therefore clear that reasonable agreement with the tracking could only be achieved when this distribution was considered. Owing to the limited computing power and the long time interval in which we were interested, the beam could only be represented by a small number of particles which we chose to be 180. We call them “superparticles” because each of them should represent a certain range in horizontal betatron amplitude r and momentum deviation $\delta = \Delta p/p$. The vertical distribution is treated only approximately. The concept of “superparticles” has to be used with some caution. In Ref. [20] it was shown that particles even close by may have very different survival times. To study this in more detail we considered 640 particles, started them in a very small phase space region, and determined their loss time, the distribution of which is shown in Fig. 25. The maximum loss is reached soon after an initial period free of losses. This maximum is followed by a very long tail which resembles an exponential decrease. The representation of a certain region in phase space with a “superparticle” introduces therefore an error which is disregarded in the following.

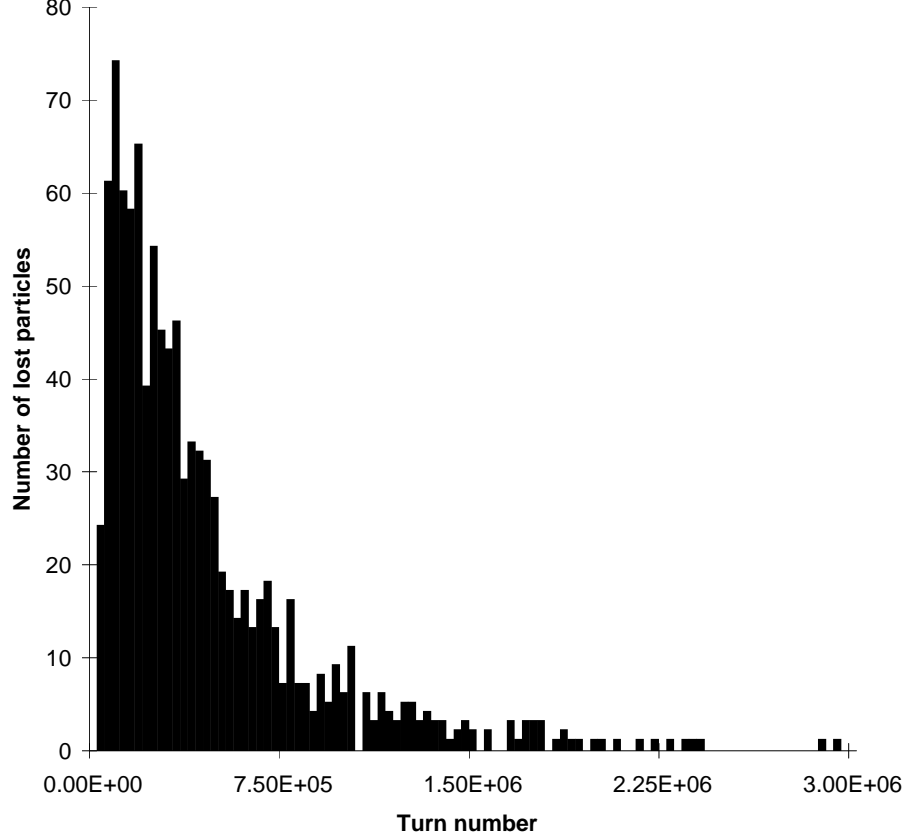


Figure 25: Distribution of survival times. Shown is the distribution of a sample of 640 particles initially placed in a small region of phase space. WP1 was used with a horizontal start amplitude of 16.0 mm (at $\beta_x = 100$ m) and a tune modulation of 40 Hz and $\Delta Q_x = 1.1 \times 10^{-3}$.

An intensity weight is assigned to each “superparticle” according to its initial position in the measured particle distribution $f(r, \delta)$. The simulated time-dependent intensity is derived by deducting from the initial intensity the weight of a “superparticle” when it is lost.

In the tracking the particles were started at a location of the machine where the dispersion is small. We therefore may factorize the distribution $f(r, \delta)$ as $f_r(r)f_\delta(\delta)$. For the horizontal betatron distribution $f_r(r)$ we assumed a Gaussian distribution with standard deviation σ before the kick. This assumption was justified by wire scan profiles. Neglecting nonlinear phase space distortions this leads to a distribution

$$f_r(r) = \frac{r}{\sigma^2} \exp\left\{-\frac{a^2 + r^2}{2\sigma^2}\right\} I_0\left(\frac{ar}{\sigma^2}\right), \quad (9)$$

after a kick a , where I_0 is the modified Bessel function of first kind and order zero. The distribution $f_\delta(\delta)$ of the momentum deviation $\delta = \Delta p/p$ is represented by

$$f_\delta(\delta) = \frac{2}{\pi} \cos^2\left(\frac{\pi}{2} \frac{\delta}{\delta_{\max}}\right). \quad (10)$$

To verify the assumption of Eq. (9) we multiplied the detuning curve $Q_x(r)$ (cf. Fig. 20) with the distribution $f_r(r)$ after a kick (σ being obtained from a fit to a wire scan profile before the kick, and a derived from the calibrated kick strength) and compared the

result with the longitudinal tune distribution obtained from the transverse Schottky signal [see Fig. 26 (a)]. The overall agreement is satisfactory with the exception of a peak that is due to the collective movement of particles in the 5th order resonance islands. Furthermore, at large amplitudes [left-hand side of Fig. 26 (a)] the experimental Schottky signal is reduced since particles have already been lost at those amplitudes. The momentum distribution $f_\delta(\delta)$ as depicted in Fig. 26 (b) agrees well with the longitudinal Schottky signal.

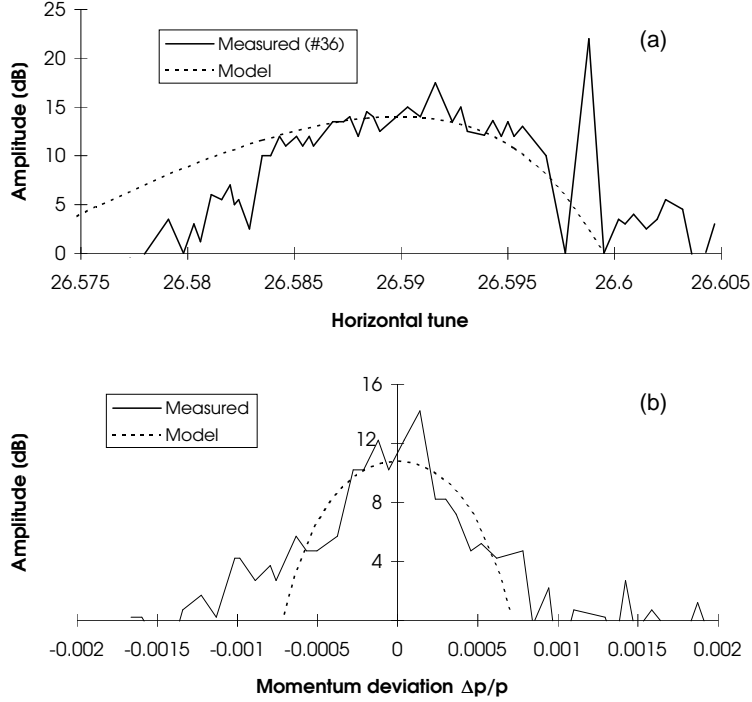


Figure 26: Comparison between measured and theoretical distribution functions.

The “superparticles” were started with initial conditions (r_m, δ_n) with $m = 0, 1, \dots, 35$ and $n = -2, -1, \dots, 2$ and the assigned weights were computed as

$$w_{mn} = \int_{r_1}^{r_2} f_r(r) dr \int_{\delta_1}^{\delta_2} f_\delta(\delta) d\delta, \quad (11)$$

$(r_1, r_2, \delta_1, \delta_2)$ being defined below. To have a better resolution close to the beam edge the step size in amplitude was reduced and the integration borders for r in Eq. (11) were computed as

$$r_1 = \begin{cases} 0 & \text{if } m = 0, \\ \frac{1}{2}(r_{m-1} + r_m) & \text{if } m > 0, \end{cases} \quad r_2 = \begin{cases} \frac{1}{2}(r_m + r_{m+1}) & \text{if } m < 35, \\ r_{\max} & \text{if } m = 35, \end{cases} \quad (12)$$

where r_{\max} is given by the scraper position. For the momentum distribution a constant step size $\Delta\delta = 2.5 \times 10^{-4}$ was chosen and the integration borders for δ were

$$\delta_1 = \begin{cases} -\delta_{\max} & \text{if } n = -2, \\ \left(n - \frac{1}{2}\right) \Delta\delta & \text{if } n > -2, \end{cases} \quad \delta_2 = \begin{cases} \left(n + \frac{1}{2}\right) \Delta\delta & \text{if } n < 2, \\ \delta_{\max} & \text{if } n = 2. \end{cases} \quad (13)$$

In the tracking the three relevant time intervals (T_{-2}, T_{-1}) , (T_{-1}, T_0) and (T_0, T_1) were treated separately. The complete intensity curve was then reconstructed by properly matching the three time intervals.

There are various types of errors. The first comes from the lack of statistics since we track 180 weighted particles instead of about 10^{12} particles in the experimental distribution.

Furthermore we use a certain number of experimental values for the reconstruction of the intensity curves, all measured with a certain precision. To estimate the effect of these errors on the simulated intensity curves we varied the values under consideration, typically by 5%. The results are listed in Table 5. The total error is given as the square root of the sum of squares of the individual errors (last row in Table 5).

Table 5: Error evaluation for the intensity curves

	$\Delta Q_x = 5.5 \times 10^{-4}$	$\Delta Q_x = 1.1 \times 10^{-3}$
Emittance ϵ	+3%/ - 6%	+3%/ - 6%
Momentum width δ_{\max}	+1%/ - 3%	+2%/ - 5%
Kick strength α	+6%/ - 6%	+10%/ - 10%
Scraper position	+3%/ - 12%	+3%/ - 11%
Total	+8%/ - 15%	+8%/ - 17%

4.2.3 Results

Out of the six cases studied with the two modulation depths ($\Delta Q_x = 5.5 \times 10^{-4}$, 1.1×10^{-3}) and for the three modulation frequencies (9 Hz, 40 Hz, 180 Hz) two are shown in Fig. 27. The reconstructed normalized intensity curve is depicted together with an experimental run.

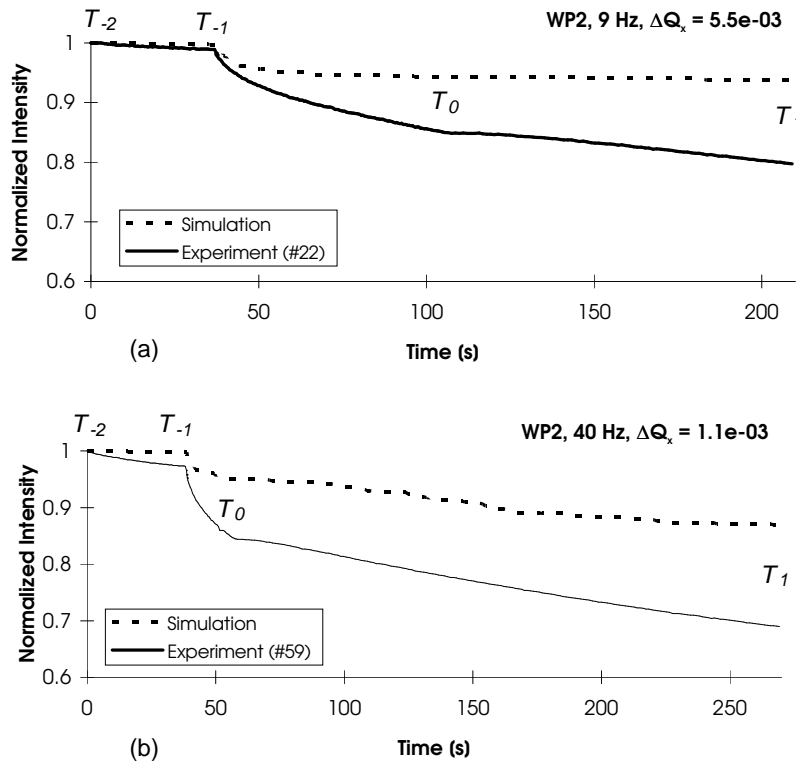


Figure 27: Measured and intensity curves reconstructed from simulations.

Besides the above-stated statistical error there is clearly a systematic underestimation of the losses and loss rates for all six tracking cases. As an example, the experimental intensities in the two cases shown in Fig. 27 at T_1 are lower compared with the simulations by 15% and 22% in part (a) and part (b), respectively.

5 THE WIRE SCANNER EXPERIMENT

Besides employing the scrapers, which are by nature destructive, as a beam observation tool, there is also the possibility in the SPS to use the almost nondestructive scanner system with the 8 μm flying wires (see Sec. 3.1.2) for the dynamic aperture studies. In the former experiments only the intensity was recorded, while in these more refined investigations the time evolution of the beam profile was the object of study. The wire scanner profiles are the projections of the particle distribution in phase space onto the x - and z -axis, respectively, and their time evolution allows a deeper insight into particle loss mechanisms. In particular the time-dependent bottom width of those profiles gives information to be compared with survival plots obtained from simulations. It must be mentioned that the scrapers were still needed as an experimental tool: firstly, they allow a definition of the beam edge and, secondly, once taken out to a larger amplitude, they serve as a known physical aperture limiter.

Taking advantage of the experience from the scraper experiment, which showed that the variation of the modulation frequency had hardly any effect on the loss rates, we restricted this new campaign of studies to a single modulation frequency of 9 Hz. The influence of the modulation depth on the particle stability was much more pronounced and we used for both working points a modulation depth which caused well-detectable particle losses (i.e. $\Delta Q_x = 1.87 \times 10^{-3}$ at WP1 and $\Delta Q_x = 0.55 \times 10^{-3}$ at WP2, respectively).

A detailed study of the beam profile evolution is given. The results of dynamic aperture measurements will be shown for both working points, with and without additional tune modulation, and compared with long-term tracking simulations. A phenomenological description of the observed beam behavior, based on tracking results and analytical estimates, will be given in Sec. 6.

5.1 Beam profile measurements

For this set of experiments the following procedure was used: at first the horizontally kicked beam was freed from vertical beam tails using a vertical scraper. Then the beam was scraped horizontally by moving the scraper to an *inner* position. Thereafter this scraper was retracted to an *outer* position to study the processes leading to particle losses in between those two scraper positions. After this scraper procedure the additional tune modulation was switched on and horizontal beam profiles were taken about every minute for typically 15 minutes. Figure 28 shows the first and last scan of such a run.

On account of the two scraper positions, we used two different setups: firstly, the *inner* scraper position was fixed and the *outer* position was varied and, secondly, the *inner* position was varied and the *outer* position was kept fixed.

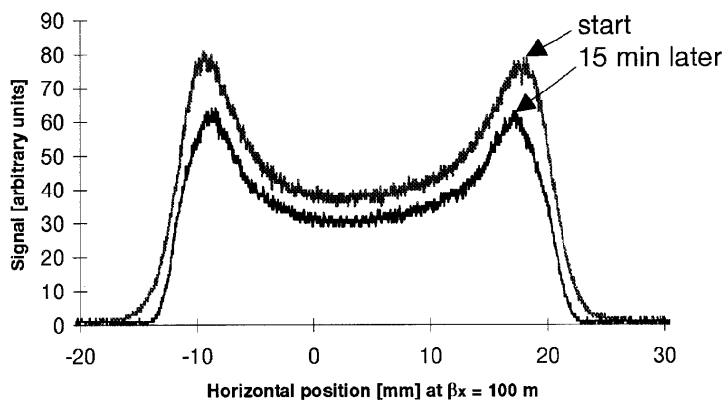


Figure 28: Time evolution of a wire scan profile.

5.1.1 First working point - WP1

Part (a) and part (b) of Fig. 29 show the half beam width and the normalized intensity of the first setup with the fixed *inner* scraper position (18 mm) while (c) and (d) were obtained with a fixed *outer* position (26 mm). Moreover, there is one horizontally unscrapped run denoted by #78. In each setup there is one case, #62 and #76 respectively, with almost identical conditions. This may serve as a reference to compare the two situations. In the first setup particle transport phenomena above 18 mm are studied while in the second setup amplitudes below 18 mm are investigated. In all legends the values given in millimeters are the differences between the *inner* and the *outer* scraper position normalized to $\beta_x = 100$ m. An estimate of the measurement precision has been attached to the cases #64 and #77. The band borders that are visible in part (c) will be discussed in Sec. 6.

In the *outer* regime [Fig. 29 (a)] the beam width remains constant for all cases after a slight drop occurring over the first 100 s. The normalized intensity [part (b)] also evolves rather similarly in all cases leading to a difference of not more than 2% after a period of 650 s. We conclude that in this regime the amplitude growth is too fast to lead to any sizable differences between the tested scraper positions.

In the *inner* regime [Fig. 29 (c)] the beam width is strongly reduced over the first 150 s of the unscrapped run (#78). It stays almost constant for the intermediate cases (#76, #77, #80) and it increases appreciably for the low-amplitude run (#82). Disregarding the first 150 s, the changes of the half beam widths evolve slowly over a long period of 600 s. In the cases at larger amplitudes this width is slightly decreasing and at lower amplitudes it is slightly increasing. After 800 s four cases almost merge at the same amplitude while the width in the lowest amplitude case is still somewhat smaller but seems slowly to approach this value as well. The normalized intensity varies strongly for the first 150 s but thereafter the lifetime is approximately the same in all cases.

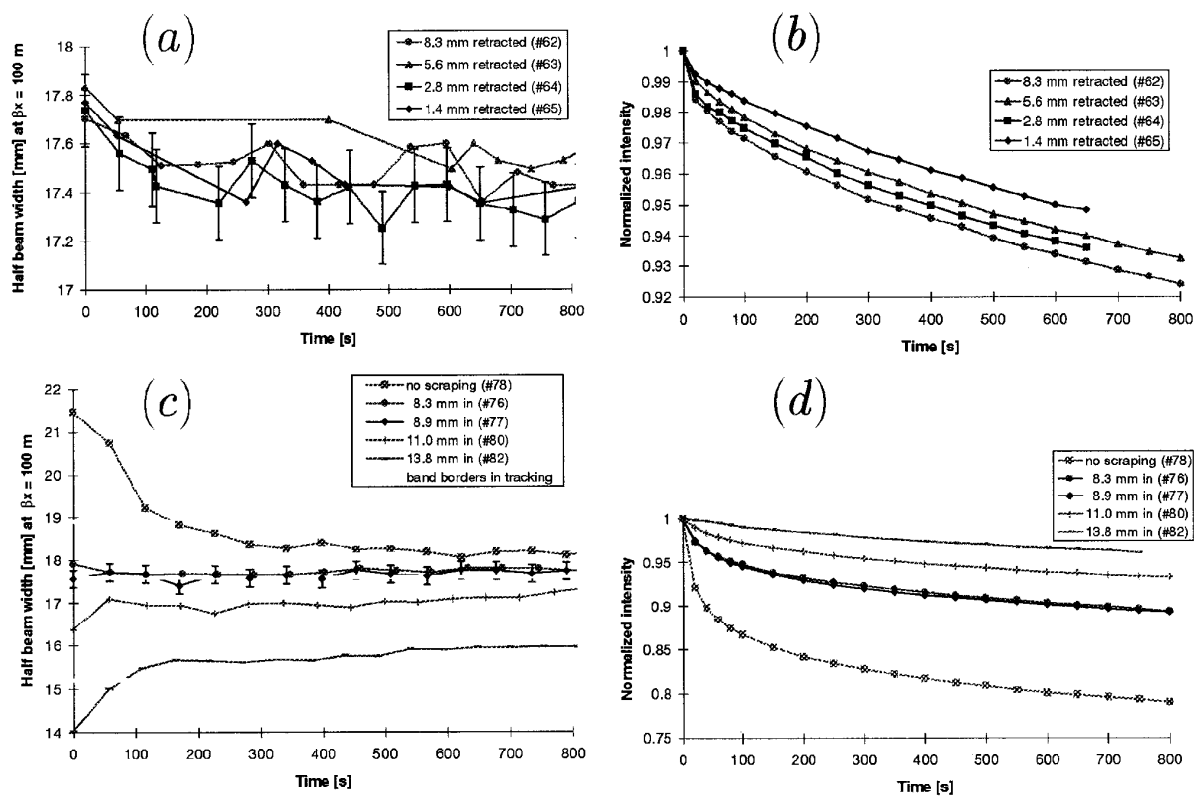


Figure 29: Wire scanner measurements at WP1.

5.1.2 Second working point - WP2

At the second working point the two setups are similar to those of working point WP1. However, the *inner* scraper position in the first setup (larger amplitude regime) is slightly larger (19 mm). Part (a) and part (b) of Fig. 30 represent again the regime of large amplitudes while parts (c) and (d) show the lower amplitude regime. The runs #66 and #83 are the reference cases for WP2 and therefore made under similar conditions.

In the *outer* regime all cases concerning half beam width and normalized intensity have a very similar behavior. Compared with the first working point, however, the motion seems considerably more unstable resulting in a decreasing width of the beam over at least the first 600 s. Note also that at this working point a four times smaller tune modulation depth was applied.

In the *inner* regime the half beam widths also seem to tend to the same value after 800 s, however, the merging process is less pronounced than that of WP1. The normalized intensities [part (d)] have not reached a regime of stabilized lifetimes as was the case at WP1.

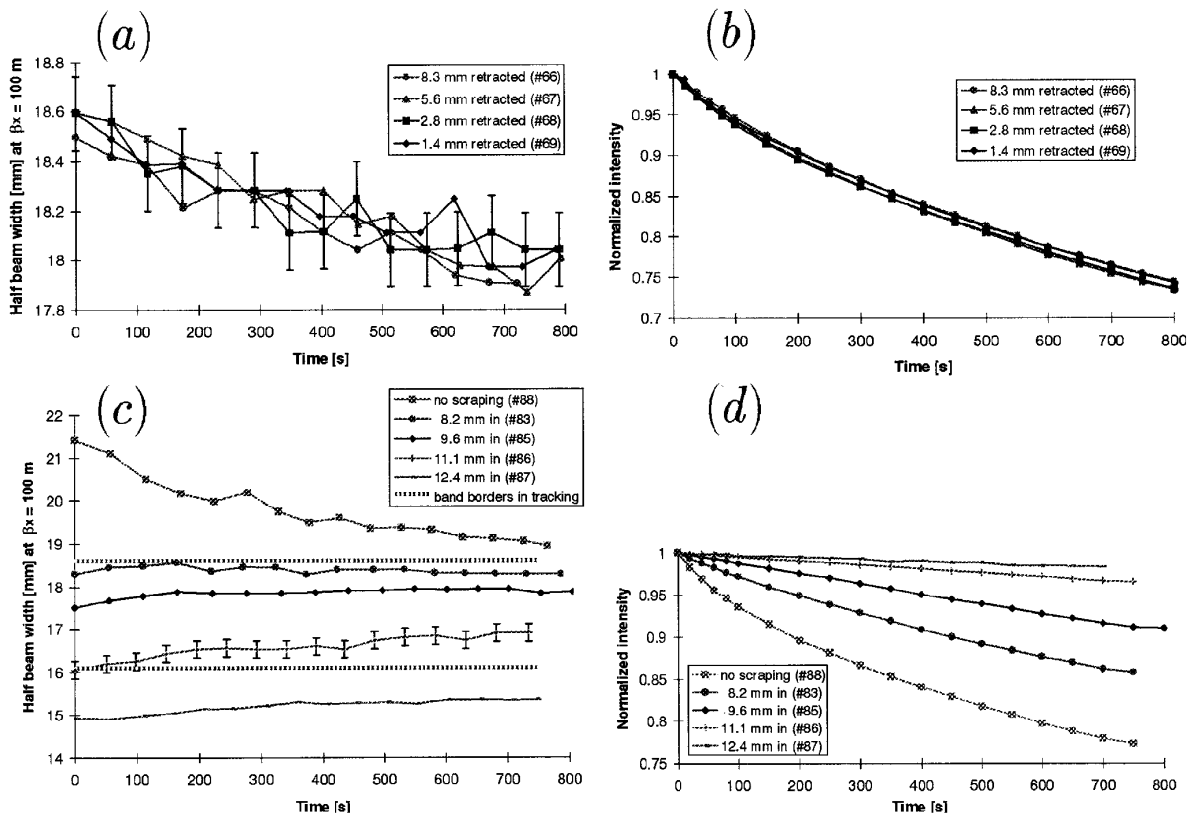


Figure 30: Wire scanner measurements at WP2.

5.2 Dynamic aperture

In the field of nonlinear accelerator dynamics various definitions of the dynamic aperture are in use. A relevant definition for machine operation is the amplitude below which no sizable particle losses take place for a time interval of interest. The dynamic aperture is a particular concern for the LHC at injection time when nonlinearities and beam size are at their maximum. Particles have to survive under these unfavorable conditions for about 15 minutes. The main practical aim of the SPS experiment was to test if tracking simulations can predict the dynamic aperture of a machine in conditions similar to those of the LHC, as far as nonlinearities are concerned.

In our studies we had to face two principal limitations: firstly, the full time interval of interest (15 min storage time or 40 million turns in the SPS) could not be fully explored with tracking simulations, only one third (345 s) could be reached with reasonable computing effort. Secondly and more relevantly, the SPS experiment was rather restricted by the large natural beam size. This precludes any fine exploration of the phase space as is done in tracking by varying the amplitude in small steps. In particular, small chaotic regions within an otherwise stable region cannot be detected. However, the maximum amplitude above which no particles survive after a certain time gives a good measurement of the stability limit.

Experimentally, the dynamic aperture is determined by using the maximum bottom width of the wire scan profiles (Fig. 28). In this section we will discuss the experimental curves shown in Fig. 31 which also depict the results from tracking to be treated in the next section.

In Fig. 31 (a) four wire-scan measurements at WP1 with additional tune modulation are displayed. These curves have been smoothed and the estimated error bars are shown in case #91. The reproducibility of the experimental results has been found to be within 2% for two measurements performed under the same conditions but five months apart (#62 and #76). Owing to the rather large beam size the results depend on the measurement procedure: cases #62 and #76 were scraped horizontally after kicking, whereas cases #78 and #91 were left unscraped and in addition the latter case was kept for some extra 15 min without additional tune modulation. Although these cases strongly differ initially, after 345 s the differences reduce to about 5%.

Figure 31 (b) shows the situation for WP2 where the applied ripple depth was about four times smaller. Two cases (#72 and #74) are not scraped, case #82, which was scraped horizontally, shows the interesting feature of the beam size growing at first and then shrinking again. Also at WP2 the differences between the various cases after 345 s are largely reduced (less than 3%).

Finally Figs. 31 (c) and (d) show the experimental results with natural ripple only. The results of all measured cases are summarized in Table 6.

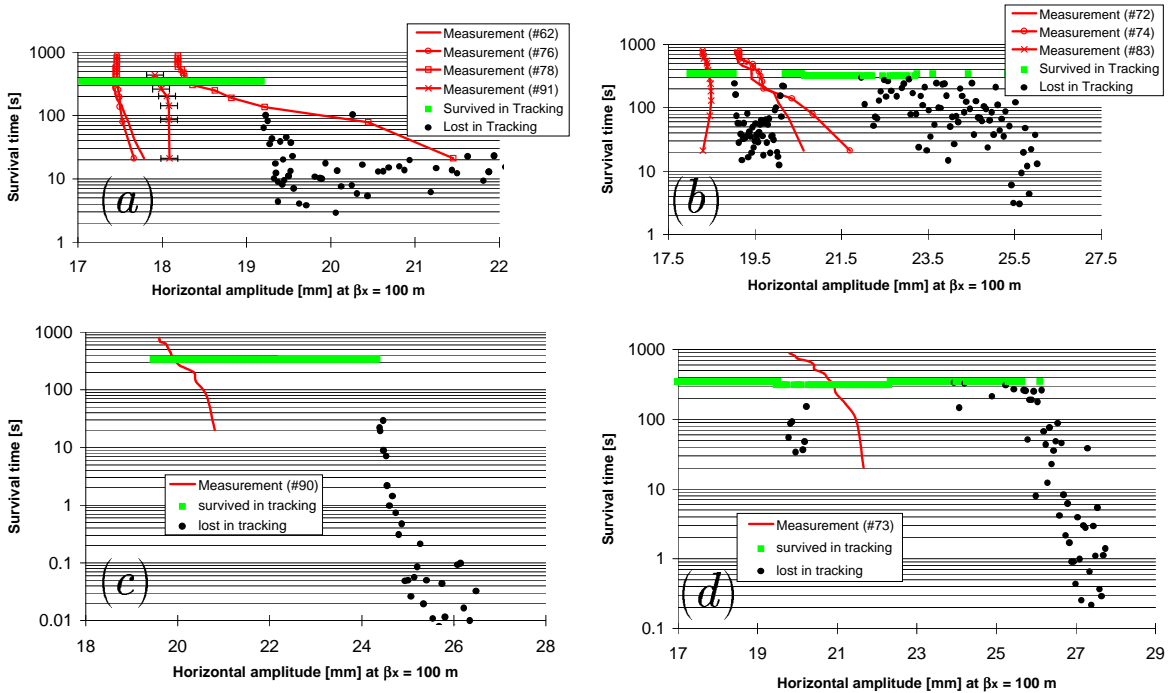


Figure 31: SPS dynamic aperture studies. Measurement and computational results for the dynamic aperture with and without additional tune ripple at WP1 are shown in (a) and (c), respectively. The situation at WP2 is depicted by (b) and (d) with and without additional tune modulation.

Table 6: Comparison of measured and computed dynamic aperture. All values are given for $\beta_x = 100$ m. For the onset of chaos there are two values: the larger one is the border above which no regular particles could be found, the lower (in brackets) is the lowest amplitude at which large-scale chaotic motion sets in.

Case	Measured dynamic aperture (mm)	Onset of chaos (2×10^5 turns) (mm)	Loss border (1.5×10^7 turns) (mm)	Comparison between measurement and loss border (%)
WP1, 9 Hz, $\Delta Q_x = 1.87 \times 10^{-3}$	17.4	(7.7) 14.3	19.2	10
WP2, 9 Hz, $\Delta Q_x = 0.55 \times 10^{-3}$	19.5	(7.4) 8.3	22.3	14
WP1, natural ripple only	20.0	(15.7) 23.1	24.4	22
WP2, natural ripple only	20.9	(9.8) 23.6	25.7	23

5.2.2 Computed

As described in Sec. 3.3, survival plots are used to compute the dynamic aperture. According to the experimental conditions, the particles are tracked with large horizontal displacements while a vertical displacement of roughly one σ of the vertical beam size was considered.

In this experiment, where relatively large tune modulations are present, the onset of chaos is a much too pessimistic indicator for long-term stability. In all tracked cases a wide amplitude range could be found (column three in Table 6) where chaotic (after 200 000 turns) and regular regions alternate. For each chaotic region in that amplitude range a particular sum resonance is found which apparently causes the unstable behavior. At WP1 [Fig. 31 (a)] the lost particles correspond to a coupled 7th order resonance or [Fig. 31 (c)] to a horizontal 13th order resonance. At WP2 [Figs. 31 (a) and (d)] the losses at large amplitudes correspond to a horizontal 7th order resonance and the losses at about 20 mm are due to another coupled 7th order resonance. These resonances can be found in Fig. 18.

The dynamic aperture, computed as explained, is shown in column four in Table 6 and the last column in this table shows the difference in percent between the computed and the measured dynamic aperture. In the cases with additional tune modulation, the difference is about 10%, but without ripple this agreement deteriorates by about a factor of two. Moreover, in the tracking we find a broad region of apparently regular motion outside the experimental stability border (not present in the cases with additional tune modulation). From this we have to conclude that an essential destabilizing effect is missing in our tracking model. A very rough estimate for the scale of this effect is given by the strength of the additional tune modulation because the experimental dynamic aperture without extra tune modulation agrees well with that of the tracking when this ripple is introduced (cf. the last two entries in column two with the first two entries in column four of Table 6). The missing effect also corresponds to the final lifetime in Fig. 29 (d) that is reached at all amplitudes; in tracking, no losses can be found at the lower amplitudes. The nature of this effect is still unknown. However, both neglected systematic nonlinearities and extra tune modulation are unlikely candidates. The former would lead to measurable

detuning with amplitude, while for the latter the tune modulation can be understood from the measured voltage ripple of the SPS power supplies [39] and in addition it has been measured with good precision with a phase-locked loop. Some more discussion of possible causes can be found in Ref. [35].

In a complementary experiment at the HERA proton ring, the dynamic aperture was measured under normal operating conditions at injection energy. Rest-gas monitors were used for the beam profile measurements. The difference between measured and computed dynamic aperture amounts to values similar to those in the SPS [7] given that the experimental conditions were well understood.

6 PHENOMENOLOGY OF CHAOTIC PARTICLE MOTION

One of the main purposes of the aperture studies was to further our phenomenological understanding of the intricate nature of the particle motion in phase space, thus continuing earlier studies [20]. In particular we were interested in the chaotic regime generated by the interplay of nonlinearities and harmonic tune modulation.

The simulation studies at WP1, based on the methods described in Sec. 3.3, are presented in the first section. The subsequent section describes experimental results that successfully demonstrate an interesting phenomenon first found in the tracking.

6.1 Simulation results

For working point WP1 and a tune modulation of 9 Hz and $\Delta Q_x = 1.87 \times 10^{-3}$ we studied three betatron amplitudes (16.8, 18.8 and 19.5 mm at $\beta_x = 100$ m) close to the long-term dynamic aperture. All sum, skew, and difference resonances in the amplitude regime of interest are shown up to order 13 in Fig. 32.

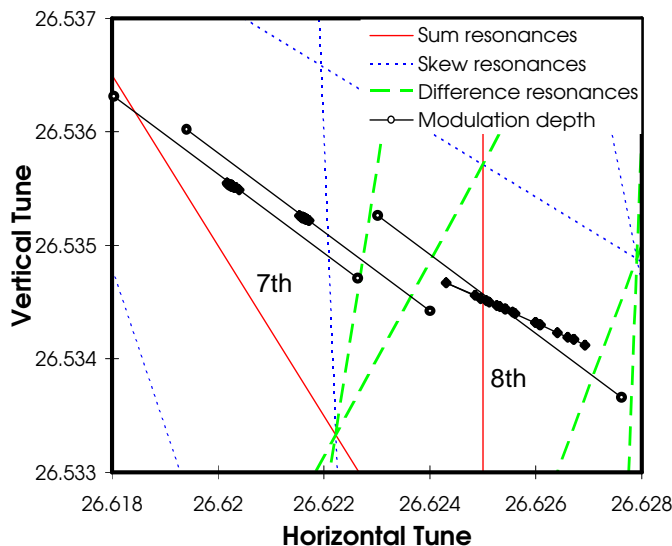


Figure 32: Tune diagram and detuning with amplitude WP1.

In the tracking studies the particle stability was tested with three methods. Firstly, we computed the angular distance of a pair of initially close-by particles after 20 000 turns (Table 7) and we found the most chaotic behavior at the smallest amplitude. Secondly, we followed the tunes averaged over one modulation period (5000 turns) for one particle. Twenty tune values so obtained at each of the three amplitudes are depicted in Fig. 32 together with the tune modulation depth. At the smallest amplitude (rightmost in Fig. 32)

the 8th order resonance is crossed due to the tune modulation leading to large fluctuations of the averaged tunes. The presence of this resonance also explains the strong chaotic behavior found with the first method. The largest amplitude (leftmost in Fig. 32) just reaches the 7th order resonance beyond which strong particle loss takes place. Note that the tunes follow closely the detuning curve shown in Fig. 19. Thirdly, we started 640 particles with initial conditions distributed over a very small phase space region at each of the three amplitudes and tracked them for 3 million turns. It is necessary to consider such distributions rather than single particles on account of the chaotic nature of the motion in the studied amplitude range in phase space.

Table 7: Particle stability at three different starting amplitudes

Horizontal amplitude (mm) at $\beta_x = 100$ m	16.8	18.8	19.5
Separation angle (π) of 2 particles after 20 000 turns	0.9	0.45×10^{-4}	0.8×10^{-3}
Lost particles out of 640	0	102	502
Amplitude rms value (mm) after 1.5 million turns	0.82	0.29	0.28

The amplitude evolution for the three starting amplitudes is shown in Fig. 33 using 32 of the 640 particles. The amplitudes are averaged over one tune-modulation period. At the lowest amplitude [Fig. 33 (c)] the particles quickly fill (less than 10^5 turns) an amplitude band around the 8th order resonance and stay within the band. The width of this band could be identified as the amplitude region of overlapping sidebands due to the tune modulation with 9 Hz and $\Delta Q_x = 1.87 \times 10^{-3}$ [35]. Not one particle out of 640 was lost (Table 7). For the second amplitude [18.8 mm, Fig. 33 (b)] the amplitudes spread slowly (10^5 – 10^6 turns). Eventually they either reach the 7th order resonance, after which they are extracted in some 10^4 turns, or they are attracted *down to the 8th order resonance*: in Fig. 33 (b) several particles show a decrease in their amplitude after 1.9 million turns to occupy an amplitude range which corresponds to that of part (c). The particles starting at 19.5 mm [Fig. 33 (a)] fill the same band as the particles starting at 18.8 mm. But since they start very close to the upper-band border, most particles are lost and only a few are attracted to the 8th order resonance.

Figure 34 shows the evolution of the amplitude rms values for the three cases. The very chaotic particles starting at 16.8 mm show an immediate increase of the rms value which is not present in the other cases. For these amplitudes the rms values are only given up to 1.7 million and 2.7 million turns, respectively, since thereafter a sizable loss or attraction to the 8th order resonance sets in which perturbs the evolution of the rms value.

Our observations of the chaotic particle motion in the phase space can be summarized as follows: at small amplitudes there is a band of strongly chaotic particles, which nevertheless survive for very long periods. This band is separated from a region of larger amplitudes where individual particles either slowly grow or decrease their betatron amplitude until they reach the bounds of the band. Finally, beyond a certain amplitude, a rapid particle loss takes place. It must be mentioned that a band structure was also found at WP2. This scenario is in clear contradiction with a global diffusion model. However, the amplitude evolution in time may be appropriately described by using, firstly, a separate (amplitude-dependent) diffusion coefficient for each band, and, secondly, transition probabilities between these bands.

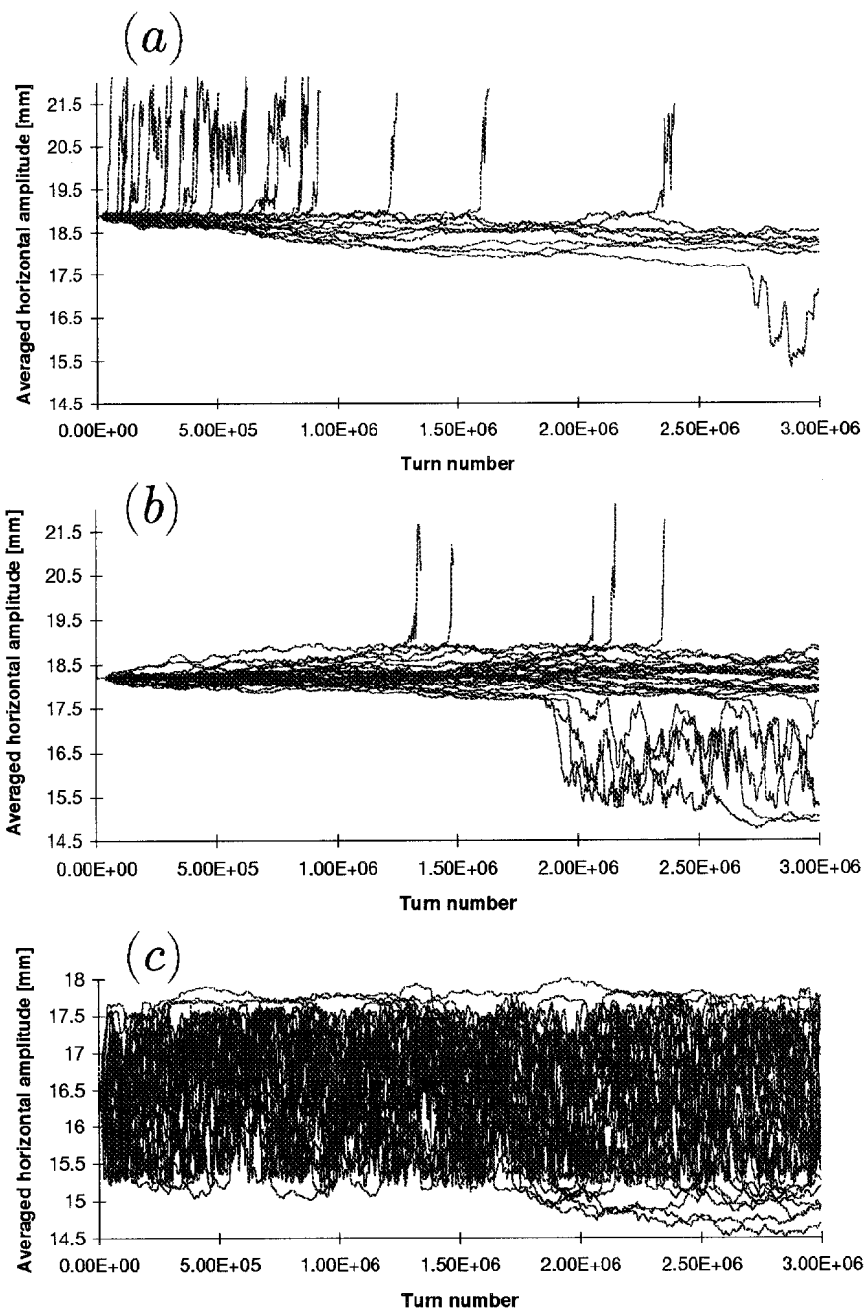


Figure 33: Amplitude evolution of particle distributions.

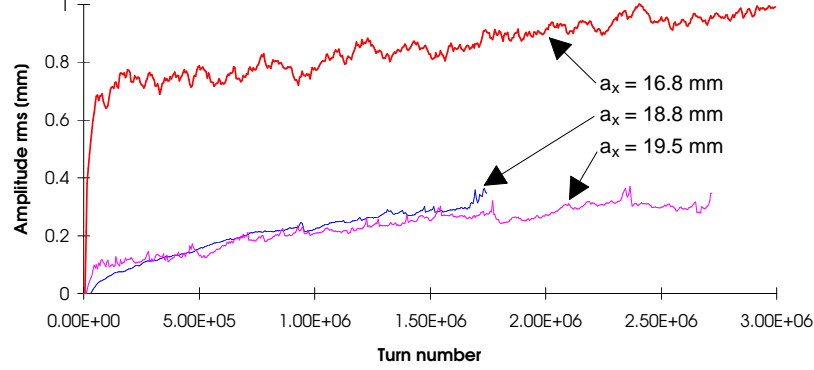


Figure 34: Time-dependent amplitude rms values. (The same amplitudes are chosen as in Fig. 33.)

6.2 Experimental observations

The first prediction from the tracking is the very existence of those bands. They are shown as thick grey lines in Figs. 29 (c) and 30 (c) for WP1 and WP2, respectively. The experimental data seem to be consistent with our phenomenological picture: the half beam width decreases in the outer band and increases in the lower band for WP1. At WP2 only one clear band could be identified in the tracking. Above this band the half beam width decreases in the experiment while inside and below this band the width stays constant or increases slightly.

The second prediction is the attraction of particles towards lower amplitudes at WP1, which is clearly visible in Fig. 33 (b). Owing to a large amplitude distribution this effect may, however, be screened by a considerable intensity loss as seen for instance in Fig. 28. It is therefore mandatory to scrape the beam tails so that the particles in the region of fast losses are removed but a sufficient number of particles remain in the amplitude band seen in parts (a) and (b) of Fig. 33. This type of experiment could be set up in the SPS and the result is shown in Fig. 35. The double-peak structure of a wire scan profile is shown right after the kick and 15 min later. The interesting feature is the shifting of the peaks *down to smaller amplitudes* without a reduction in peak height. This can only be interpreted as the predicted decrease of amplitude of a sizable fraction of the beam. This observation is not a singular event but was found in four separate experimental runs.

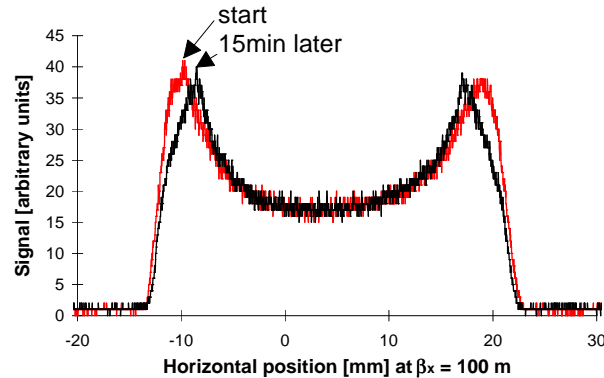


Figure 35: Decreasing of the betatron amplitudes of a sizable fraction of the beam at WP1 (#65).

In 1993 we concluded the experiments intended to measure transport coefficients of particles in the chaotic regime by using scrapers to remove beam tails and limit the physical aperture. Despite a very careful preparation of the beam and the instrumentation it was not possible to obtain reproducible quantitative results. The qualitative results of earlier experiments could, however, be well reproduced: the loss rates increase with increasing tune modulation depth, and there is practically no dependence of the loss rates on the tune modulation frequency in the range from 9 Hz to 180 Hz. Two simultaneous modulation frequencies have a larger effect than a single one, and these experimental results are in qualitative agreement with theoretical expectations.

In 1994 dynamic aperture measurements were done using the evolution of wire scan profiles. In the presence of strong tune modulation ($\Delta Q_x = 1.87 \times 10^{-3}$) the dynamic aperture could be reproduced with tracking simulation with a precision of 10%. Without additional tune modulation this agreement deteriorates to some 20%. We conclude that we have still not identified an important effect which is masked by the strong tune modulation.

In parallel, tracking simulations were performed with a view to extending our phenomenological understanding of the details of chaotic particle motion. An interesting outcome is the finding that the degree of chaoticity is not a good indicator for the survival time. There is also evidence from simulations and experiment that sizable fractions of particle distributions can move to smaller amplitudes. Moreover, a simple continuous diffusion model can be excluded for the description of the overall loss mechanism. Instead, a more complex model is needed which allows for sudden changes in the behavior of the particle motion when certain borders are reached in phase space.

Acknowledgements

We wish to thank our colleagues from the accelerator physics group for participation in the experiment and discussions on the results, in particular J. Gareyte, W. Herr, J. Miles, and V. Ziemann. W. Scandale and T. Linnecar made an important contribution to the experiment in measuring the tune ripple spectrum.

Essential to the success of the experiment was, of course, the help of the operations team: X. Altuna, C. Arimatea, R. Bailey, R. Billen, G. Buur, K. Cornelis, G. Crockford, B. Desforges, C. Despas, A. Faugier, A. Ferrari, R. Giachino, L. Normann, G. Robin and A. Spinks.

The data acquisition system was made operational and maintained by the following persons from the beam instrumentation group: A. Burns, H. Jakob, I. Milstead and L. Vos. A data visualization program was provided by A. Sweeney and G. Morpurgo. The linear wire scanner system was adapted to our needs by J. Camas, G. Crockford, G. Ferioli, J.J. Gras, R. Jung and J. Koopman. The kicker was kept operational and calibrated with the help of E. Carlier and L. Ducimetière. We thank M. Laffin for calibrating the scrapers and D. Bakker for technical support.

Special thanks go to F. McIntosh for his continuous performance improvements of the computing facilities and programs.

Nevertheless, it seems doubtful [41] whether such a simple criterion can be blindly applied when very weak effects can lead to a reduction of the long-term dynamic aperture. For the LHC design we therefore follow a somewhat more conservative approach: the detuning criterion of $\Delta Q < 0.005$ is kept and the “smear” is used as a measure of how much the amplitude varies in phase. Fulfilling the former criterion allows one to achieve an acceptable dynamic aperture, especially when the detuning correction is done quasi-locally in each half-cell. Of course some detuning is needed to stabilize other instabilities, but in practice it is just about possible to get the detuning down to the desired values [42]. The “smear”, on the other hand, has become an essential complement to the dynamic aperture that is usually determined by keeping the phases at fixed values and finding the amplitudes at which the motion is just stable. For those amplitudes the “smear” gives a measure of the amplitude variations along the phase coordinates. The time-consuming variation of initial phases can therefore be avoided and the stable fraction of the beam in phase space can be much better evaluated.

- [1] H. Brück, R. Meinke, and P. Schmüser, “Methods for magnetic measurements of the superconducting HERA magnets,” *Kerntechnik* **56**, 248–256 (1991).
- [2] E. W. Collins *et al.*, contribution to the Topical Workshop on Magnetic Effects of Persistent Currents in Superconductors, Fermilab, 1990;
H. Brück *et al.*, “Time dependence of persistent-current field distortions in the superconducting HERA magnets,” in *Proceedings of the Second European Particle Accelerator Conference*, Nice, 1990, edited by P. Marin and P. Mandrillon (Ed. Frontières, Gif-sur-Yvette, 1990).
- [3] T. Linnecar and W. Scandale, “Phenomenology and causes of the 50 Hz spaced lines contaminating the Schottky signals,” SPS Improvement Report 203, CERN SPS/DI-MST/TL/WS/EEK (1986);
L. Evans and J. Gareyte, “Beam–Beam Effects,” in *CERN Advanced Accelerator School*, Oxford, 1985, edited by S. Turner (CERN, Geneva, 1987), CERN 87–03.
- [4] J. Gareyte, “Experimental evidence of transverse nonlinear phenomena in accelerators,” *Part. Accel.* **27**, 187–196 (1990).
- [5] D. A. Edwards and M. J. Syphers, “Experimental particle tracking,” in *Third US–CERN School on Particle Accelerators*, Anacapri, 1988, edited by M. Month and S. Turner (Springer, Berlin, 1989), Lecture Notes in Physics, Vol. 343, pp. 222–240.
- [6] J. Gareyte, W. Scandale, and F. Schmidt, “Review of the dynamic aperture experiment at the CERN SPS,” in *International Workshop on Nonlinear Problems in Accelerator Physics*, Berlin, 1992, edited by M. Berz, S. Martin, and H. Ziegler (Institute of Physics, Bristol, 1993), Inst. Phys. Conf. Ser. No. 131, pp. 235–248.
- [7] O. Brüning *et al.*, “A comparison of measured and calculated dynamic aperture of the HERA proton ring at injection energy,” DESY HERA 95–05 and CERN/SL/95–69 (AP) (1995).
- [8] A. Chao *et al.*, “Experimental investigations of nonlinear dynamics in the Fermilab Tevatron,” *Phys. Rev. Lett.* **61**, 2752–2755 (1988);
S. G. Peggs, “Hamiltonian theory of the E778 nonlinear dynamics experiment,” presented at the *Second Advanced ICFA Beam Dynamics Workshop on Aperture-Related Limitations of the Performance and Beam Lifetime in Storage Rings*, Lugano, 1988, edited by J. Hagel and E. Keil (CERN, Geneva, 1988), CERN 88–04;
D. A. Edwards and M. J. Syphers, “An overview of experiment E778,” in *Second Advanced ICFA Beam Dynamics Workshop on Aperture-Related Limitations of the Performance and Beam Lifetime in Storage Rings*, Lugano, 1988, edited by J. Hagel and E. Keil (CERN, Geneva, 1988), CERN 88–04, pp. 95–144;
N. Merminga, “An experimental study of the SSC magnet aperture criterion,” presented at the *First European Conference on Particle Accelerators*, Rome, 1988, edited by S. Tazzari (World Scientific, Singapore, 1989);
N. Merminga, “A study of nonlinear dynamics in the Fermilab Tevatron,” Ph. D. thesis, University of Michigan, 1989;
T. Chen *et al.*, “Measurements of a Hamiltonian system and their description by a diffusive model,” *Phys. Rev. Lett.* **68**, 33–36 (1992);
T. Satogata *et al.*, “Driven response of a particle beam,” *Phys. Rev. Lett.* **68**, 1838–1841 (1992);
T. Satogata, “Nonlinear resonance islands and modulational effects in a proton synchrotron,” Ph. D. thesis, Northwestern University, 1993.

- [9] J. Y. Liu *et al.*, “Determination of the linear coupling resonance strength using 2d invariant tori,” *Phys. Rev. E* **49**, 2347–2352 (1994);
 Y. Wang *et al.*, “Effects of tune modulation on particles trapped in 1D resonance islands,” *Phys. Rev. E* **49**, 5697–5705 (1994);
 M. Ellison *et al.*, “Experimental measurements of a betatron difference resonance,” *Phys. Rev. E* **50**, 4051–4062 (1994).
- [10] S. Y. Lee, “Review of nonlinear beam dynamics experiments,” paper presented at the *International Workshop on Nonlinear Problems in Accelerator Physics*, Berlin, 1992, edited by M. Berz, S. Martin, and H. Ziegler (Institute of Physics, Bristol, 1993), *Inst. Phys. Conf. Ser. No. 131*.
- [11] J. Bridge *et al.*, “Dynamic aperture measurements on Aladdin,” *Part. Accel.* **28**, 1–9 (1990);
 E. Crosbie *et al.*, “Non-linear resonance studies at the Synchrotron Radiation Center, Stoughton, Wisconsin,” in *Particle Accelerator Conference*, San Francisco, 1991, edited by L. Lizama and J. Chew (IEEE, New York, 1991);
 J. Liu *et al.*, “Difference resonance study on the electron storage ring Aladdin at SRC,” *Part. Accel.* **41**, 1–41 (1993).
- [12] P. Tran *et al.*, “Nonlinear beam dynamics experimental program at SPEAR,” SLAC-PUB-95-6720 (1995).
- [13] R. L. Evans *et al.*, “Non linear dynamic aperture experiments, 1 Oct., 21 Oct., 5 Nov. 1986,” CERN SPS/AMS/JG, SPS Improvement Report No. 209, 1986;
 A. Hilaire, “Dynamic aperture at the SPS,” presented at the *Second Advanced ICFA Beam Dynamics Workshop on Aperture-Related Limitations of the Performance and Beam Lifetime in Storage Rings*, Lugano, 1988, edited by J. Hagel and E. Keil (CERN, Geneva, 1988), CERN 88-04;
 L. R. Evans *et al.*, “The non linear dynamic aperture experiment in the SPS,” CERN SPS/88-22 (AMS), in *First European Conference on Particle Accelerators*, Rome, 1988, edited by S. Tazzari (World Scientific, Singapore, 1989), pp. 619–621.
- [14] K. Cornelis *et al.*, “Effect of sextupoles on the single particle dynamics in the CERN SPS,” CERN SPS/88-45 (AMS), LHC Note 85;
 F. Schmidt, “Tracking results with SIXTRACK for the 1988 dynamic aperture experiment,” CERN SPS/88-49 (AMS);
 J. Gareyte, A. Hilaire, and F. Schmidt, “Dynamic aperture and long-term particle stability in the presence of strong sextupoles in the CERN SPS,” CERN SPS/89-2 (AMS), presented at the *Particle Accelerator Conference*, Chicago, 1989, edited by F. Bennett and J. Kopta (IEEE, New York, 1989).
- [15] D. Brandt *et al.*, “First Results of the diffusion experiment,” CERN SL/AP/NOTE/90-5;
 D. Brandt *et al.*, “Influence of power supply ripple on the dynamic aperture of the SPS in the presence of strong nonlinear fields,” CERN SL/90-67 (AP), LHC Note 126, in *Second European Particle Accelerator Conference*, Nice, 1990, edited by P. Marin and P. Mandrillon (Ed. Frontières, Gif-sur-Yvette, 1990), pp. 1438–1440;
 X. Altuna *et al.*, “The 1991 dynamic aperture experiment at the CERN SPS,” CERN SL/AP 91-43, LHC Note 171, in *Advanced ICFA Beam Dynamics Workshop on Effects of Errors in Accelerators, their Diagnosis and Corrections*, Corpus Christi, 1991, edited by A. W. Chao (AIP, New York, 1992), AIP Conf. Proc. No. 255, *Particles and Fields No. 48*, pp. 355–369.

- [16] A. Gerassimov, "The applicability of diffusion phenomenology to particle losses in hadron colliders," CERN SL/92-30 (1992), FERMILAB-Pub-92/185.
- [17] M. Furman and F. Schmidt, "Reduction of the dynamic aperture due to tune modulation," CERN SPS/89-1 (AMS), SSCL-A-6.
- [18] D. A. Edwards, F. Schmidt, and M. J. Syphers, E778 experiment in 1989, private communication.
- [19] O. S. Brüning, "Diffusion in a FODO cell due to modulation effects in the presence of non-linear fields," Part. Accel. **41**, 131-151 (1993);
O. Brüning, "An Analysis of the Long-Term Stability of the Particle Dynamics in Hadron Storage Rings", Ph. D. thesis, Hamburg University, DESY 94-085 (1994).
- [20] F. Galluccio and F. Schmidt, "Towards a better understanding of slow particle losses in large hadron colliders," CERN SL/91-44 (AP), LHC Note 172, in *Advanced ICFA Beam Dynamics Workshop on Effects of Errors in Accelerators, their Diagnosis and Corrections*, Corpus Christi, 1991, edited by A. W. Chao (AIP, New York, 1992), AIP Conf. Proc. No. 255, Particles and Fields No. 48, pp. 86-104.
- [21] T. Linnecar and W. Scandale, "Continuous tune measurements using the Schottky detector," CERN SPS/83-19 (DI-MST), in *10th Particle Accelerator Conference*, Santa Fe, 1983 [IEEE Trans. Nucl. Sci. **NS30** (4), pt. 2, (1983)].
- [22] A. Burns *et al.*, "The BOSC project," CERN SL/90-68 (AP), presented at the *Second European Particle Accelerator Conference*, Nice, 1990, edited by P. Marin and P. Mandrillon (Ed. Frontières, Gif-sur-Yvette, 1990);
A. Burns *et al.*, "The million turn data acquisition system BOSC," in *Conference Record of the 1993 IEEE Particle Accelerator Conference*, Washington, D.C., 1993, pp. 2301-2303;
- [23] I. Milstead and H. Jakob, "SPS BOSC System User Guide," CERN SL/Note 95-114 (BI);
W. Fischer and F. Schmidt, "Application software for BOSC," CERN SL/Note 93-64 (AP) (1993).
- [24] W. Herr, "M.O.P.S. users guide for 'C' programs," CERN SPS/88-43(AMS) (1988);
Q. King and R. Schmidt, "The SPS catalogue data structure," CERN SPS/ABM/Note/88-12 (1988).
- [25] A. Sweeney, "The dataviewer programmer's guide," LEP controls note 107, SPS/ACC Note 89-11 (1989);
G. Morpurgo, "The SL/CO dataviewer on HP-UX," CERN SL/BI internal note (1994).
- [26] A. Sweeney, private communication.
- [27] F. Schmidt, "Smear calculation in the presence of linear coupling for the 1988 dynamic aperture experiment," CERN SPS/88-50 (AMS);
M. A. Furman and S. G. Peggs, "A Standard for the Smear," SSC-N-634, 1989;
J. Bengtsson and J. Irwin, "Analytical Calculations of Smear and Tune Shift," SSC-232 (1990).
- [28] J. Bosser *et al.*, "Transverse emittance measurement with a rapid wire scanner at the CERN SPS," Nucl. Instrum. Methods Phys. Res. **A235**, 475-480 (1985), CERN SPS/84-11 (1984);
J. Bosser *et al.*, "The micron wire scanner at the SPS," CERN SPS/86-26 (MS) (1986);
A. Burns *et al.*, "Wire scanner news from the CERN-SPS," CERN SPS/89-13 (1989),

- presented at the *Particle Accelerator Conference*, Chicago, 1989, edited by F. Bennett and J. Kopta (IEEE, New York, 1989) .
- [29] G. Crockford, private communication.
 - [30] J. Gareyte, private communication.
 - [31] G. Ripken, “Non-linear canonical equations of coupled synchro-betatron motion and their solution within the framework of a non-linear 6-dimensional (symplectic) tracking program for ultrarelativistic protons,” DESY 85–084 (1985);
D. P. Barber, G. Ripken, and F. Schmidt, “A non-linear canonical formalism for the coupled synchro-betatron motion of protons with arbitrary energy,” DESY 87–036 (1987);
F. Schmidt, “SIXTRACK, version 1.2, single particle tracking code treating transverse motion with synchrotron oscillations in a symplectic manner,” CERN SL/94–56 (AP) (1994), found in WWW under:
<http://hpariel.cern.ch/frs/Documentation/doc.html>.
 - [32] F. Willeke, “Analysis of particle tracking data,” in *Proceedings of the Third Advanced Accelerator Physics Course*, Uppsala, 1989, edited by S. Turner (CERN, Geneva, 1990), CERN 90–04;
F. Schmidt, “SIXTRACK - a single particle tracking code,” in *Proceedings of the Workshop on Nonlinear Problems in Future Particle Accelerators*, Capri, 1990, edited by W. Scandale and G. Turchetti (World Scientific, Singapore, 1991).
 - [33] F. Schmidt, “Untersuchungen zur dynamischen Akzeptanz von Protonenbeschleunigern und ihre Begrenzung durch chaotische Bewegung,” Ph. D. thesis, Hamburg University (in German), DESY HERA 88–02 (1988);
L. Schachinger and Y. Yan, “Recent SSC dynamic aperture measurements from simulations,” SSC–N–664 (1989).
 - [34] T. Bell *et al.*, “CERN’s PaRC workstation cluster for engineering computing,” CERN CN/94/8, May 1994.
 - [35] W. Fischer, “An experimental study on the long-term stability of particle motion in hadron storage rings,” Ph. D. thesis, Hamburg University, to be published.
 - [36] A. Schoch, “Theory of linear and nonlinear perturbations of betatron oscillations in alternating gradient synchrotrons,” CERN 84–15 (1984).
 - [37] R. Brinkmann and F. Willeke, “Chromatic corrections and dynamic aperture in the HERA electron ring, part I,” DESY 86–079 (1986).
 - [38] M. Seidel, “Determination of diffusion rates in the proton beam halo of HERA,” DESY HERA 93–04 (1993);
M. Seidel, “The proton collimation system of HERA,” DESY 94–103 (1994).
 - [39] P. Burla *et al.*, “Power supply ripple study at the SPS,” CERN SL/94–11 (AP) (1994), in *Accelerator Physics at the Superconducting Super Collider*, Dallas, TX, 1992–1993, edited by Y. T. Yan, J. P. Naples, and M. J. Syphers (AIP, New York, 1995), AIP Conf. Proc. No. 326.
 - [40] A. Chao, “Accelerator physics studies for the SSC,” IEEE Trans. Nucl. Sci. **NS32**, 3442–3446 (1985).
 - [41] É. Forest, private communication.
 - [42] M. Giovannozzi, W. Scandale, and F. Schmidt, “Tune-shift correction for LHC version 2 using Normal Forms,” CERN SL/93–29 (AP), LHC Note 230.